

**Measurement and Prediction of  $pK_a$  of Linear and Cyclic Amines Using Group-Additivity  
and Artificial Neural Network (ANN) Models**

A Thesis

Submitted to the Faculty of Graduate Studies and Research

In Partial Fulfillment of the Requirements

For the Degree of

Master of Applied Science

In

Industrial Systems Engineering

University of Regina

By

Venkata Sai Priyatham Varma Alluri

Regina, Saskatchewan

January, 2022

Copyright © 2022: V. Alluri

**UNIVERSITY OF REGINA**  
**FACULTY OF GRADUATE STUDIES AND RESEARCH**  
**SUPERVISORY AND EXAMINING COMMITTEE**

Venkata Sai Priyatham Varma Alluri, candidate for the degree of Master of Applied Science in Industrial Systems Engineering, has presented a thesis titled, ***Measurement and Prediction of pKa of Linear and Cyclic Amines Using Group-Additivity and Artificial Neural Network (ANN) Models***, in an oral examination held on January 6, 2022. The following committee members have found the thesis acceptable in form and content, and that the candidate demonstrated satisfactory knowledge of the subject material.

External Examiner:                   \*Dr. Saman Azadbakht, Petroleum Systems Engineering

Supervisor:                           \*Dr. Amr Henni, Industrial Systems Engineering

Committee Member:                 \*Dr. Hussameldin Ibrahim, Industrial Systems Engineering

Committee Member:                 \*Dr. Ezeddin Shirif, Industrial Systems Engineering

Chair of Defense:                   \*Dr. Saqib Khan, Faculty of Business Administration

\*via ZOOM Conferencing

## Abstract

This research is focused on the estimation of dissociation constants ( $pK_a$ ) of eight amines, namely: 3-(Diethylamino) propylamine, 1,3-Diaminopentane, 3-Butoxypropylamine, 2-(Methylamino) ethanol, Bis (2-methoxyethyl) amine,  $\alpha$ -Methylbenzylamine, 2-Aminoheptane, 3-Amino-1-phenylbutane in the temperature range of 293.15K to 323.15K using the potentiometric titration method. The van't Hoff equation was used to estimate the standard state enthalpy change ( $\Delta H^0$ ) and standard state entropy ( $\Delta S^0$ ).

$pK_a$  values were predicted using the Perrin–Dempsey–Serjeant (PDS) functional additivity model, the modified PDS and the Qian, Sun, Sun, and Gao (QSSG) model. The obtained root mean square (RMS) errors for the three models were 0.41, 0.25 and 0.17, respectively.

$pK_a$  values of amines that have significant importance in the process of  $CO_2$  capture were predicted using an Artificial Neural Network (ANN) model, with the help of a back-propagation algorithm. Ten variable parameters were used as input data in this estimation, which were further broadly divided into 3 subcategories, namely: 1) The properties that are used to identify the compound are considered as the inputs such as the molecular weight, numbers of H atoms, N atoms, C atoms and O atoms; 2) The properties that were used to correlate the  $pK_a$  values were the temperature, density, viscosity, refractive index, and sound velocity. Finally, the experimentally determined  $pK_a$  values were considered as the output. The density, viscosity, refractive index and sound velocity of the eight amines under study were experimentally determined in this work. The detailed experimental procedure was also reported. The developed architecture consisted of 10 inputs, 40 neurons in the first hidden layer and 39 neurons in the second hidden layer, and a single output parameter leading to a model with 10-40-39-1 parameters. This model was found to be very efficient in predicting the  $pK_a$  of amines not

included in the training database. The regression coefficient was 0.90755 and the mean squared errors for training, validation and testing were  $MSE_{\text{train}} = 0.0069$ ,  $MSE_{\text{validation}} = 0.037$  and  $MSE_{\text{test}} = 0.0597$ , respectively.

To reduce the complexity of the model, another architecture with a structure of 8-40-39-1 was developed. Density and viscosity values remained as inputs, which led to a slightly lower regression coefficient of 0.89225 and higher mean squared errors  $MSE_{\text{train}} = 0.00881$ ,  $MSE_{\text{validation}} = 0.02945$  and  $MSE_{\text{test}} = 0.0789$ . With just two parameter representing the physical and transport properties of the amines, the complexity of the system was greatly reduced, but it was still able to predict accurately the  $pK_a$  values of amines .

## **Acknowledgements**

I would love to express my sincerest gratitude to my supervisor, Dr. Amr Henni, for his constant support and guidance throughout the tenure of my research. I could not have imagined having a better advisor and mentor for my Master's thesis. His patience, knowledge and insights truly helped me in the due process.

Besides my supervisor, I would also like to thank my thesis committee: Dr. Saman Azadbakht, Dr. Ezeddin Shirif, Dr. Hussameldin Ibrahim, and Dr. Saqib Khan for their encouragement, insights and valuable feedback.

I would also like to acknowledge the teaching and support provided by Dr. William (Hoang Chi Hieu) Nguyen and Poojan Vyas. I also would like to extend my thanks to Krishna and Jahnavi for their constant support and for always believing in me.

I am very grateful for the support and love of my parents and sibling without whom this entire journey would have not been possible.

## Table of Contents

<b>Abstract</b> .....	<b>i</b>
<b>Acknowledgements</b> .....	<b>iii</b>
<b>List of Figures</b> .....	<b>vi</b>
<b>List of Tables</b> .....	<b>viii</b>
<b>Chapter 1 : Introduction</b> .....	<b>1</b>
1.1 Emissions and policies .....	1
1.2 Carbon Capture and Storage (CCS) .....	4
<b>Chapter 2 : Literature Review</b> .....	<b>9</b>
2.1 CO <sub>2</sub> capture based on amine-based absorption.....	9
2.2 Significance of pK <sub>a</sub> .....	11
2.3 Scope .....	11
<b>Chapter 3 : Experimental procedure and PDS prediction of pK<sub>a</sub> of amines</b> .....	<b>13</b>
3.1 Introduction .....	13
3.2 Apparatus and chemicals required.....	14
3.3 Experimental procedure.....	16
3.4 Results & Observations .....	17
3.5 PDS prediction of pK <sub>a</sub> values for protonated amines .....	29
<b>Chapter 4 : pK<sub>a</sub> Predictions of Amines using Artificial Neural Network (ANN)</b> .....	<b>34</b>
4.1 Introduction .....	34
4.2 Background and Overview of ANN .....	35
4.2.1 Feed-forward Neural Network.....	36
4.2.2 Backpropagation algorithm.....	37

4.3 Data aggregation and variable selection.....	39
4.4 ANN Model and Observations .....	42
4.4.1 Model with all recorded input parameters .....	42
4.4.2 Model with optimized input parameters .....	48
<b>Chapter 5 : Conclusion.....</b>	<b>55</b>
<b>References.....</b>	<b>57</b>
<b>Appendix A: Experimental Determination of Physical Properties of Amines .....</b>	<b>65</b>
Appendix A-1: Density Measurement.....	65
Appendix A-2: Viscosity Measurement .....	66
Appendix A-3: Refractive Index Measurement.....	67
Appendix A-4: Sound Velocity Measurement .....	68
<b>Appendix B: Weights and Bias of different layers in ANN.....</b>	<b>69</b>
Appendix B-1: Weights and bias for the model with all input parameters. ....	69
Appendix B-2: Weights and bias for the model with optimized inputs. ....	71

## List of Figures

Figure 1.1 Global CO <sub>2</sub> emissions based on total consumption.....	1
Figure 1.2 CO <sub>2</sub> emissions worldwide in the year 2020 .....	2
Figure 1.3 Geological CO <sub>2</sub> storage resources (in millions of tonnes) .....	6
Figure 1.4 Various CO <sub>2</sub> capture technology originating from energy conversion .....	7
Figure 3.1 A comparative plot of titration curves at different temperatures for MEA .....	19
Figure 3.2 Comparative analysis of ionization constants of MEA between a specified range of temperatures of 298.15K and 313.15K.....	20
Figure 3.3 ln (Ka1) vs 1000/T f (a) all amines; (b) primary amines; and (c)secondary amine ....	24
Figure 3.4 ln (Ka) vs 1000/T for studied amines. (a) ln (Ka1)for monoamines (b) ln (Ka2) of diamines .....	25
Figure 4.1 The basic ANN architecture .....	35
Figure 4.2 ANN architecture used in this work .....	36
Figure 4.3 ANN performance with respect to varying number of neurons in the first hidden layer. (i) R; (ii) MSE. ....	44
Figure 4.4 ANN performance with respect to varying number of neurons in the second hidden layer. (i) R; (ii) MSE. ....	45
Figure 4.5 Final ANN architecture for pKa prediction. ....	46
Figure 4.6 Performance of ANN with different epochs (MSE).....	46
Figure 4.7 Scatter plot for the regressive prediction of pKa.....	47
Figure 4.8 Zero-line representation in an error histogram.....	48
Figure 4.9 Enhanced performance of the model with respect to the optimized input parameters.	50
Figure 4.10 Scatter plot for the regressive prediction of pKa for the new model.....	51

Figure 4.11 Error histogram of the optimized ANN model.....	52
Figure 4.12 pKa prediction for amine 1.....	53
Figure 4.13 pKa prediction for amine 2.....	53
Figure 4.14 pKa prediction for amine 3.....	54

## List of Tables

Table 2.1 Widely used amines commercially used for CO <sub>2</sub> capture .....	10
Table 3.1 List of amines used in this experimental work .....	15
Table 3.2 Experimentally determined pH values of buffer solutions at specific temperatures .....	16
Table 3.3 Debye-Hückel equation constants for aqueous solution.....	18
Table 3.4 pK <sub>a</sub> value of MEA at 298.15 K .....	19
Table 3.5 pK <sub>a1</sub> values of the studied amines at different temperatures .....	21
Table 3.6 pK <sub>a2</sub> values for the two diamines at different temperatures .....	22
Table 3.7 Standard state enthalpy change and entropy change of the first pK <sub>a</sub> of the studied amines .....	26
Table 3.8 Standard Gibbs-Free energy of reaction for the first pK <sub>a</sub> of the studied amines at various temperatures .....	27
Table 3.9 Standard state enthalpy change and entropy change of the second pK <sub>a</sub> of the studied amines .....	28
Table 3.10 Standard Gibbs-Free Energy of Reaction for the Second pK <sub>a</sub> of the Studied Amines at Various Temperatures .....	28
Table 3.11 pK <sub>a</sub> prediction using PDS, new PDS and QSSG methods.....	30
Table 3.12 PDS method .....	31
Table 3.13 New PDS method.....	32
Table 3.14 QSSG method .....	32
Table 4.1 Data aggregation for this work .....	40
Table 4.2 Comparison of different ANN models' performance.....	49

# Chapter 1 : Introduction

## 1.1 Emissions and policies

The necessity of CO<sub>2</sub> capture is of paramount importance in today's world as CO<sub>2</sub> is one of the most influential greenhouse gases (GHG). It captures the infrared radiation and causes the temperature to increase. The current increase and decrease in temperatures depending on locations and change in climatic conditions are due to global warming, which in the past few years has risen the overall temperature by approximately 2 °C. This has been one of the major reasons for the increase in precipitation, low snowfall years and heavy snowmelt in northern Canada and the western USA [1]. Even though an increasing number of governments and public associations started becoming conscious of global warming and legislated strict laws to lessen fossil fuel consumption, it is not entirely possible to find an alternative to fossil fuels yet.



Figure 1.1 Global CO<sub>2</sub> emissions based on total consumption [2]

The quantity of fossil fuels burnt yearly has been reaching a new record level every year since 1990, a break to this trend was observed in the year 2020 due to Covid -19. The change can be observed from the graphical representation provided in Figure 1.1 [2]. Similarly, the contribution to these emissions by individual nations is represented in Figure 1.2 [2].

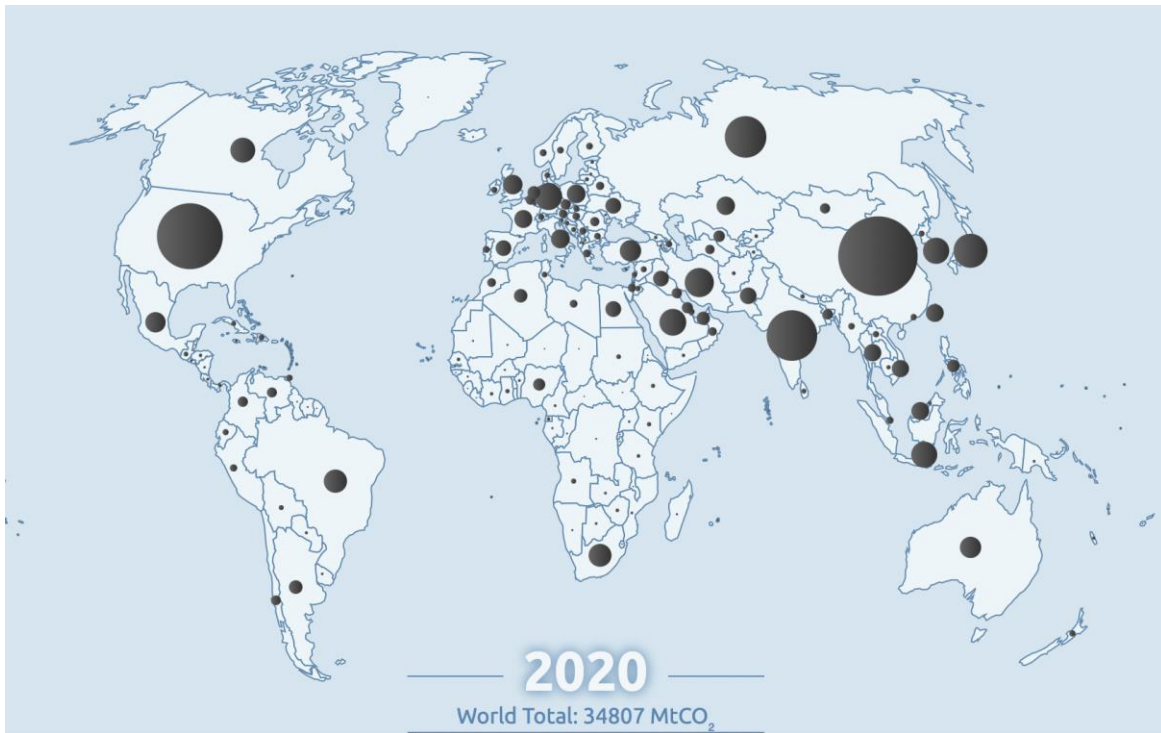


Figure 1.2 CO<sub>2</sub> emissions worldwide in the year 2020. [2]

The energy sector is the largest source of CO<sub>2</sub> emissions. One of the most carbon-intensive fuels is coal. For instance, every tonne of coal burned produces approximately 2.5 tonnes of CO<sub>2</sub> which is alarmingly high for any type of fossil fuel [3]. Due to various other factors, coal constitutes one-third of fossil fuels' share in the entire world and hence is responsible for almost 43% of CO<sub>2</sub> emissions from the use of fossil fuels [3].

The transportation sector is considered the second-largest source of CO<sub>2</sub> emissions. The transportation of people and goods produced around 22% of CO<sub>2</sub> emissions around the world by

the burning of fossil fuels [4]. This energy-intensive industry utilizes petroleum-based fuels like gasoline, diesel, kerosene etc. Since the 1990s transport-related emissions have grown at an alarming rate of 45% in less than 3 decades [4]. The aviation industry has accounted for 11% of transport-related CO<sub>2</sub> emissions. About 62% of these emissions were generated by international flights and domestic flights make up for the remainder 38% of emissions [4]. Over the last decade, aviation has become one of the fastest-growing carbon-intensive forms of transportation.

The industrial sector comes in the third position for CO<sub>2</sub> emissions. This sector is usually made up of construction, mining, manufacturing, and agriculture. The sector produces 20% of fossil fuel-related CO<sub>2</sub> emissions [3]. The manufacturing process is a major player in this sector. For instance, the production of 100kg of cement produces 900kg of CO<sub>2</sub>, and 1 tonne of steel manufactured produces 1.9 tonnes of CO<sub>2</sub> [3].

The natural sources of CO<sub>2</sub> emissions are much larger than human sources of emissions. The amount of CO<sub>2</sub> produced by natural sources is completely offset by natural carbon sinks [4]. As a result, steady levels of CO<sub>2</sub> were observed before the industrial revolution. The major contributing factors are atmospheric changes in the ocean, respiration of humans and animals, decomposition and volcanic eruptions. The overall percentages of contribution for these may be staggering but have been balanced out for thousands of years now [4].

In 2015, 195 nations signed the Paris Agreement [5, 6], whose primary goal was to restrict common worldwide temperature increase to less than 2 °C by 2050. The world is well behind the target of meeting the weather goals set out by the agreement. Due to the constant depletion of resources and increase in usage of available resources, it is about time for the governments to turn their attention to installing new CO<sub>2</sub> capture plants. To support this ambition, some governments, private and public sector organizations have refocused their efforts to further reduce CO<sub>2</sub>

emissions, after the COP-26 meeting in Glasgow [5]. Much stronger climate policies have been laid out and many companies have targeted to reduce one, two and three types of emissions. Around 50 countries, provinces or cities have pledged and committed to achieving net zero-emission by the date set by the agreement i.e., 2050 [5, 6].

## 1.2 Carbon Capture and Storage (CCS)

CCS faces numerous challenges even with today's technologically advanced world. One of the major concerns is the overall financial costs incurred during the implementation of CCS. As outlined, a CCS system broadly performs actions including but not limited to CO<sub>2</sub> capture, storage and transportation, out of which CO<sub>2</sub> capture alone is responsible for more than  $\frac{3}{4}$  of the entire incurred costs [6, 7]. Considering the brighter side of this workflow, the price of electricity produced from coal-fired power plants is predicted to rise twice the amount [8], however, the use of CCS facilities would decrease the use of combustion and effectively decrease the price of electricity by a huge margin [7, 8, 9]. This has resulted in an exponential growth in the number of R & D efforts focussed on decreasing the overall costs for CCS implementation.

According to the global status report 2020 [10], CSS facilities will be classified as follows:

- Commercial-CCS facilities: These are the facilities that would be used for CO<sub>2</sub> capture and permanent storage as part of a commercial operation.
- Pilot and demonstration facilities: These facilities hold the CO<sub>2</sub> captured for testing, developing and demonstrating the CCS technologies.

In the past decade, the CCS facility pipeline development has been quite turbulent. The total capacity of these pipelines decreased steadily between 2011 and 2017, possibly because both the public and private sectors focussed on short-term goals after they were hit by a financial crisis. Nevertheless, there has been strong growth in the past three years. [10]

A few of the milestones that the CCS industry has achieved in the past few years can be highlighted as follows [10]:

- The Alberta Carbon Trunk Line (ACTL) started its operation in March 2020 with a capacity of 14.6 Mt of CO<sub>2</sub>. It is an infrastructure that has been considered to store the highest capacity of CO<sub>2</sub> in the world [10].
- In Australia, the Gorgon Carbon Dioxide Injection Facility has been storing CO<sub>2</sub> since August 2019, it is the largest dedicated geological storage operation in the world [10].
- Quest CCS facility is the hub that captures CO<sub>2</sub> from three steam methane reformers in Alberta, Canada. In July 2020, the facility reached a total CO<sub>2</sub> storage level of 5Mt [10].

The global emission of CO<sub>2</sub> has taken a gradual increase over the past few decades, the change can be observed from the graphical representation provided in Figures 1.1 and 1.2 [2]. In early 2020, the development and deployment of CCS gained a significant boost. This was hit by Covid-19, this pandemic impacted the production which scaled back significantly. The carbon capture operation was paused in several CCS facilities and was strictly indicated to restart when the global economic conditions improve.

Many CSS projects use oil and gas fields to store their CO<sub>2</sub> as they are the most secure and proven structures that can hold huge amounts without any issues. The field of oil and gas has been majorly researched for decades and this helps in identifying any issues and also helps us respond to failures much more easily. The approximate number of CO<sub>2</sub> storage resources of major oil and gas fields is presented in Figure 1.3 [10]. The geological storage resources for CO<sub>2</sub> in saline formation are significantly greater than the storage resources of oil or gas as shown in the adjoining Figure 1.3.



Figure 1.3 Geological CO<sub>2</sub> storage resources (in millions of tonnes) [10]

In 2020, CSS was mainstreamed into energy and climate policy discussions with the support of all political parties in the Americas region. The operational CSS facilities have a capture capacity of over 30 million tonnes per annum [11]. CSS is being welcomed by numerous states and provinces. Promises to decarbonize power by different provinces have been on the rise, in both the USA and Canada. Several states are trying to achieve a zero-emission goal shortly, which would require setting up and running CSS facilities [11].

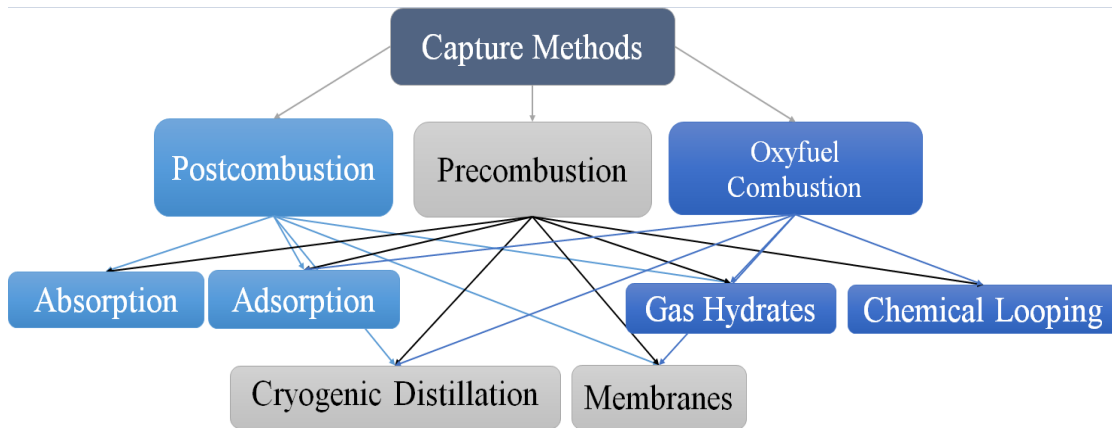


Figure 1.4 Various CO<sub>2</sub> capture technology originating from energy conversion [11]

The major source of CO<sub>2</sub> emission is the combustion of fuels for electricity production in coal-fired plants. The process of capturing the emitted CO<sub>2</sub> can be broadly classified into three groups namely, pre-combustion, post-combustion and air separation that would be followed by oxyfuel combustion [11]. The initial process of a separation typically involves either Absorption, Adsorption or Membrane. The decision is based on a set of variables that include the amount of CO<sub>2</sub> present in the gas mixture, the current chemical environment that the gas is present in and properties such as temperature and pressure etc. An outline has been described in Figure 1.4 [11].

The pre-combustion strategy mainly focuses on achieving a combustion system that is very low carbon-intense and follows the Integrated Gasification Combined Cycle (IGCC) method to achieve the same. In the case of post-combustion, an attempt to remove the CO<sub>2</sub> is done after the fuel combusts with air [12].

Absorption is considered to be the most reliable separation strategy and is widely used in industrial applications today. The organic compounds that can absorb CO<sub>2</sub> without any chemical reaction are called physical absorbents [12]. The process of physical absorption is considered to be highly beneficial if the stream pressure is high, usually above 1.4 MPa. This process allows for

the regeneration of absorbents at considerably lower energy levels, achieved by the technique of flashing [6, 11, 13]. The major drawback of physical absorption is that it is difficult to achieve a high rate of CO<sub>2</sub> removal and also a low rate of mass transfer.

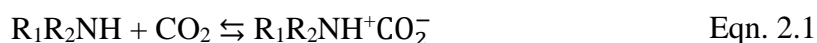
The separation of CO<sub>2</sub> from the gas is also achieved by the process of chemical absorption as it has a considerably high rate of mass transfer. The chemical reactions taking place in this process act as an additional supplementing force [1, 6, 13]. The CO<sub>2</sub> consumed is between the range of 0.4-0.7 MPa in partial pressure, which shows that low partial pressure is the most economical situation for this process. In the case of post-combustion power plants, the partial pressure observed for the mixture is approximately 0.012 MPa, leading to chemical absorption being more applicable for CO<sub>2</sub> capture as it has very low partial pressure for flue gases. The CO<sub>2</sub> gas can be treated by smaller amounts of absorbent which makes it possible to achieve a lower level of CO<sub>2</sub> concentration when compared to the process of physical absorption.

## Chapter 2 : Literature Review

### 2.1 CO<sub>2</sub> capture based on amine-based absorption

Even as technology has advanced over the decades for capturing CO<sub>2</sub>, the chemical absorption field had a considerable number of issues including high energy of regeneration and high corrosion [1, 6, 11-15]. The appropriate selection of a chemical solvent is of paramount importance in the CO<sub>2</sub> capture process. Amines' ability to react with CO<sub>2</sub> reversibly makes them the perfect fit for this process [16]. As amines are classified namely as primary, secondary and tertiary depending on the replacement of ammonia molecules with the number of hydrogen atoms. Primary amines have a limited CO<sub>2</sub> absorption capacity compared to tertiary amines because they needed more energy for regeneration, whereas tertiary amines produce bicarbonates by absorbing CO<sub>2</sub> and promoting hydrolysis. This substitutes the need for a direct chemical reaction with CO<sub>2</sub> so that the overall energy required for regeneration is less [16].

The reaction processes for primary and secondary amines are depicted through Equations 2.1 and 2.2 [17], where B is any base.



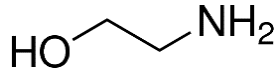
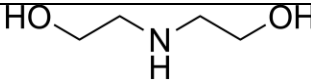
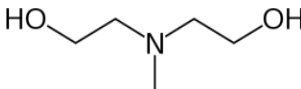
As for tertiary amines, the nitrogen bond has three substitutes so they will react with CO<sub>2</sub> only and produce bicarbonates as outlined in Equation 2.3[17].



Amines are also classified into different categories depending on the number of amino groups. If an amine has one amino group it is called monoamine and if it has two or three amino

groups, it is called di- and tri-amine, respectively. In an amino group, a nitrogen atom plays an important role in the reaction process. Alkanolamines are used for the CO<sub>2</sub> capture-based experimental process because if alkanolamines have one hydroxyl group it will increase the water solubility along with reducing vapour pressure [1]. Among all the alkanolamines commercially available, MEA, DEA and MDEA are very well known and widely used in the CO<sub>2</sub> capture process. Primary alkanolamines with hydroxyl group are the most preferred for the post-combustion CO<sub>2</sub> capture process.

Table 2.1 Widely used amines that are commercially used for CO<sub>2</sub> capture

Chemical	Type	Structure
Monoethanolamine (MEA)	Primary	
Diethanolamine (DEA)	Secondary	
Methyldiethanolamine (MDEA)	Tertiary	

The studies being conducted in the field of pK<sub>a</sub> measurement and prediction have helped understand and analyze the behaviour of these compounds under test during the chemical reaction. This knowledge has been applied in numerous fields including but not limited to physicochemical reactions, drug discovery, synthesis and analysis of compounds [18, 19]. The estimation of pK<sub>a</sub> values of amines is very significant as it helps learn more about the behaviour of amines in the process of CO<sub>2</sub> capture. Qiang et al. explored the relationship and importance of pK<sub>a</sub> of amines in the development of human and veterinary antibiotics [20]. Nath and Henni studied the efficiency of diamines to act as a solvent for CO<sub>2</sub> capture in a wide range of temperatures [21]. Joback et al. explored the influence pK<sub>a</sub> and amine structure on the overall energy consumption for the post-

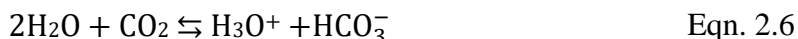
combustion CO<sub>2</sub> capture process [22]. Gao outlined a comparative analysis between pK<sub>a</sub> values that have been experimentally determined and the values determined using an ANN model [23]. Nguyen et al. proposed the use of density functional theory to optimize the geometrics after each protonation step that helps in the comparison of pK<sub>a</sub> values of amines [24].

## 2.2 Significance of pK<sub>a</sub>

According to the theory proposed by Brønsted-Lowry, an acid is defined as a substance that will be ionized into a given solution, while a base acts as a substance that will accept a hydrogen ion. In other words, it states that an acid is a proton donor and a base is a proton acceptor. This relation is explained in equation 2.4 [19].



The relative strength of the acids determines the proton separation between bases. In an amine-based absorption, CO<sub>2</sub> reacts with water leading to the formation of carbonate and bicarbonate ions as reported in equations 2.5 and 2.6 [19].



## 2.3 Scope

This work majorly focuses on the pK<sub>a</sub> determination of conjugate acids of eight novel amines at (20, 25, 30, 35, 40 and 50) °C. The potentiometric titration was used to experimentally determine pK<sub>a</sub> values. In addition to the experimental determination of pK<sub>a</sub> values, an Artificial Neural Network (ANN) model was devised to predict the pK<sub>a</sub> of amines. To assist in building a robust model, several different physical properties like Density, Viscosity, Refractive Index and Sound

Velocity of the amines were also measured experimentally at the aforementioned temperature points.  $pK_a$  values that were obtained as results from this model were compared with those obtained using the Perrin–Dempsey–Serjeant (PDS) Group-Additivity model [19], its modified version (New PDS) [39] and a model called QSSG [20].

## Chapter 3 : Experimental procedure and PDS prediction of pK<sub>a</sub> of amines

### 3.1 Introduction

There have been different studies that explore the experimental determination of pK<sub>a</sub> values which included potentiometric titration, spectrophotometry and capillary electrophoresis [16]. The most widely used method for this purpose in the case of regular amines is potentiometric titration. We utilized a pH meter to measure the values in this case. The pH meter was made of one electrode which measured the pH value of the solution into which it was inserted. The potential difference was the value that was of interest in the experiment. Based on the activity of hydrogen ions in the solution the potential of the pH electrode kept changing dynamically. The relationship between the difference in potential and the activity of hydrogen ions is given by the Nernst equation outlined in equation 3.1 [18].

$$E = -\frac{RT}{F} \ln\{H^+\} \quad \text{Eqn. 3.1}$$

Where E represented the potential in Volts, T was the absolute temperature in Kelvin, R denoted the gas constant and F represented the Faraday number.

It is very important to note that the electrodes need to be recalibrated at each temperature level as the potential measured was dependent on the change in temperature as reported in equation 3.1 [18, 26, 27]. The pH of a solution at a given temperature can be calculated using the aforementioned equation and is given in the following equation 3.2 [19].

$$\text{pH} = \log\{H^+\} = \frac{E_{\text{cell}} - E_{\text{ref}}}{A} \quad \text{Eqn. 3.2}$$

### 3.2 Apparatus and chemicals required

A total of eight amines were studied. Six were purchased from Sigma-Aldrich Canada and two were obtained from Tokyo Chemical Industries (TCI). The list of amines used along with their molecular structures, CAS Numbers and Purities are reported in Table 3.1. Monoethanolamine (MEA), was chosen to validate the instrument and experimental procedure as its pKa was well-documented in the literature. For the process of titration 0.1 M Hydrochloric acid (HCL) was purchased from Fisher Scientifics, Canada. The pH meter was manufactured by Denver Instruments (model 270 pH/ ion/ conductivity/ titration controller). Buffer solutions of 4.00 pH, 7.00 pH and 10.00 pH were purchased from VWR and their pH values were measured and reported in Table 3.2. To obtain the desired temperature and maintain it throughout the experiment the beaker was connected to a water bath and equipped with a temperature controller unit. There is a possibility that the amines may absorb small traces of CO<sub>2</sub> in the atmosphere. To prevent this from happening, pure nitrogen (purity 99.99%) was used as a blanket over the beaker for the entire experiment. This ensured that the potentiometric titration was well secured and sealed off from the atmosphere. The nitrogen used in this process was purchased from Praxair, Canada.

Table 3.1 List of amines used in this experimental work

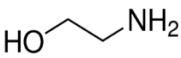
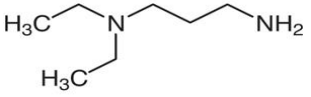
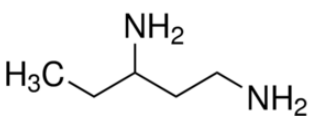
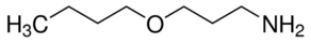
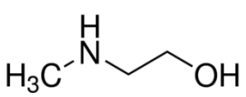
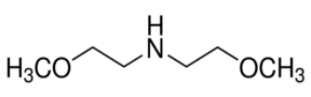
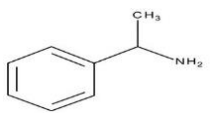
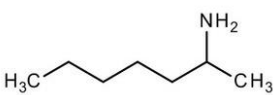
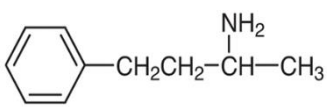
Structure	Chemical Name	CAS Number	Purity
	Monoethanolamine (MEA)	141-43-5	≥99%
	3-(Diethylamino)propylamine	104-78-9	>99%
	1,3-Diaminopentane	589-37-7	98%
	3-Butoxypropylamine	16499-88-0	99%
	2-(Methylamino)ethanol	109-83-1	≥98%
	Bis(2-methoxyethyl) amine	111-95-5	98%
	α-Methylbenzylamine	618-36-0	99%
	2-Aminoheptane	123-82-0	99%
	3-Amino-1-phenylbutane	22374-89-6	98%

Table 3.2 Experimentally determined pH values of buffer solutions at specific temperatures

T/K	pH		
	Buffer (4.00)	Buffer (7.00)	Buffer (10.00)
293.15K	4.00±0.01	7.02±0.02	10.05±0.02
298.15K	4.00±0.01	7.00±0.02	10.00±0.02
303.15K	4.01±0.01	6.99±0.02	9.95±0.02
308.15K	4.02±0.01	6.98±0.02	9.91±0.02
313.15K	4.03±0.02	6.98±0.02	9.87±0.03
323.15K	4.06±0.02	6.97±0.02	9.81±0.03

### 3.3 Experimental procedure

Initially, we needed to set the desired temperature in the water bath with the help of a thermostatic controller which brought the actual temperature inside the jacketed beaker to the desired temperature. Before the start of each experiment, we calibrated and validated the pH meter at that particular temperature using the three standard buffer solutions with known pH values and it is tabulated in Table 3.2.

An aqueous amine solution of 100 ml with a concentration of 0.01 mol/L of the studied amine was prepared at the start of every titration-based measurement with the help of double-distilled water that was produced in the lab. A quantity of 50 mL of this diluted solution was transferred into a beaker. The beaker was covered with a piece of Parafilm and a slow stream of nitrogen is passed into the beaker to ensure that the amine solution is not reacting with air which may result in deviations in the results. It is important to note that the nitrogen outlet should be above the solution and the flow of nitrogen needs to be slow and controlled.

A steady flow of 0.5 mL of HCL was gradually added to the amine solution which was being stirred at 100 rpm using a magnetic stirrer and a magnetic bar. We recorded the values at each interval of HCL addition and kept the process going forward until a gradual drop was observed. We used these values to calculate the pK<sub>a</sub> value of the specified amine at that particular temperature.

### 3.4 Results & Observations

pK<sub>a</sub> values of MEA were obtained using the same experimental process outlined in Section 3.3 and it was used for validation of the apparatus and setup of the equipment. Then the pK<sub>a</sub> values of all the amino groups (monoamines, diamines and triamines) were measured using a similar procedure.

An aqueous amine solution of MEA can be ionized and protonated to MEAH<sup>+</sup> as reported in equation 3.3, and the pK<sub>a</sub> of MEA before thermodynamic correction could be obtained using equation 3.4. [18]. pK<sub>a</sub> results would be more accurate if we corrected the results by considering the effect of the activity coefficient [18], and this step was called the thermodynamic correction (TC). The Debye-Hückel equation (equation 3.5), was used to calculate the activity coefficient [18]. The calculated activity coefficient (equation 3.6) was then used to calculate the concentration of protonated amines as shown in equation 3.7 [24].



$$\text{pK}_a^M = \text{pH} + \log \frac{[\text{MEAH}^+]}{[\text{MEA}]} \quad \text{Eqn. 3.4}$$

$$\gamma_i = \frac{-Az_1^2\sqrt{I}}{1+Bk_1\sqrt{I}} \quad \text{Eqn. 3.5}$$

$$[\text{MEA}^{\text{H}^+}] = \frac{\{\text{MEA}^{\text{H}^+}\}}{\gamma_i} \quad \text{Eqn. 3.6}$$

The constants depended on the temperature and the dielectric constants in the Debye- Hückel equation were named B and A. The charge of the ion is given by  $Z_i$ . The mean average distance of approach of ions was given by  $k_i$ . The values A and B were reported in Table 3.3 and were taken from the literature [28]. The ionic strength (I) can be calculated using Equation 3.7[18].

$$I = 0.5\sum(c_i Z_i^2) \quad \text{Eqn. 3.7}$$

Table 3.3 Debye-Hückel equation constants for aqueous solution

Temperature (K)	A ( $\text{mol}^{-1/2}\text{L}^{1/2}$ )	B ( $\times 10^8 \text{ cm}^{-1}$ )
293.15	0.5046	0.3276
298.15	0.5092	0.3286
303.15	0.5141	0.3297
308.15	0.5190	0.3307
313.15	0.5241	0.3318
323.15	0.5351	0.3341

$\text{pK}_a$  value after thermodynamic correction can be obtained by simply subtracting the TC from the raw experimental  $\text{pK}_a$  value as shown in equation 3.8[24].

$$\text{pK}_a^{\text{T}} = \text{pK}_a^{\text{M}} - \text{TC} \quad \text{Eqn. 3.8}$$

By combining all the calculated values, the determined  $pK_a$  values for MEA at 298.15K are reported in Table 3.4 and plotted in Figure 3.1. A titration curve was shown for MEA at all temperatures studied.

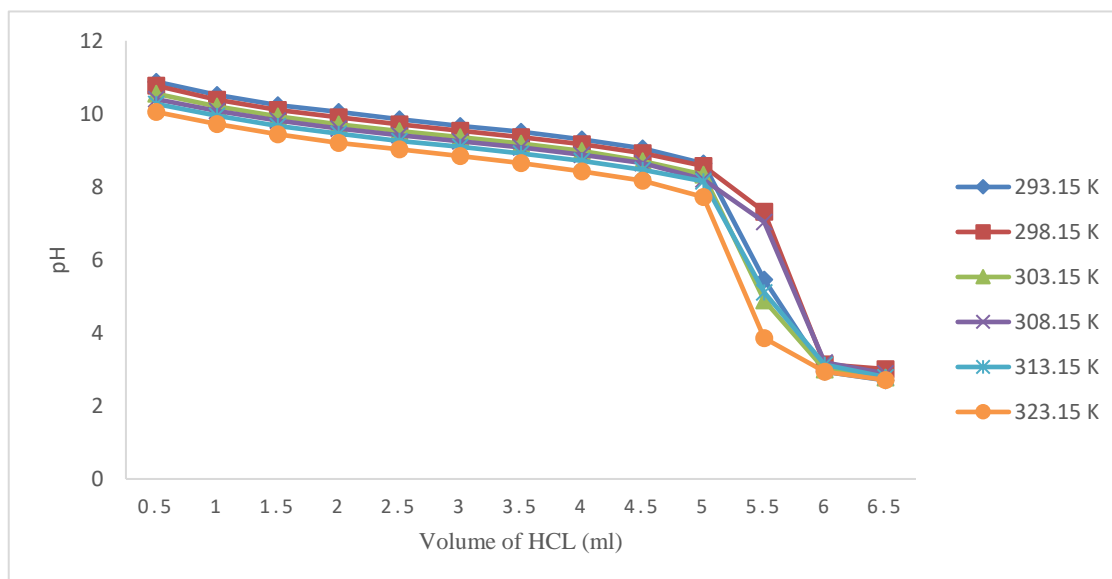


Figure 3.1 A comparative plot of titration curves at different temperatures for MEA

Table 3.4  $pK_a$  value of MEA at 298.15 K

HCL (ml)	pH	$\frac{[MEAH^+]}{[MEA]}$	$\log \frac{[MEAH^+]}{[MEA]}$	TC	$pK_a$
0.0	10.77	-	-	-	-
0.5	10.39	0.11	-0.96	0.02	9.41
1	10.11	0.24	-0.61	0.02	9.48
1.5	9.9	0.42	-0.38	0.03	9.50
2	9.71	0.65	-0.19	0.03	9.49
2.5	9.54	0.97	-0.01	0.03	9.49
3	9.36	1.44	0.16	0.03	9.48
3.5	9.17	2.21	0.34	0.04	9.48
4	8.92	3.68	0.57	0.04	9.45
4.5	8.57	7.68	0.89	0.04	9.41
5	7.32	-	-	-	-
Average					9.47

In Figure 3.2, plots are presented based on the ionization constant of MEA and a comparison between the experimental and literature values is presented.

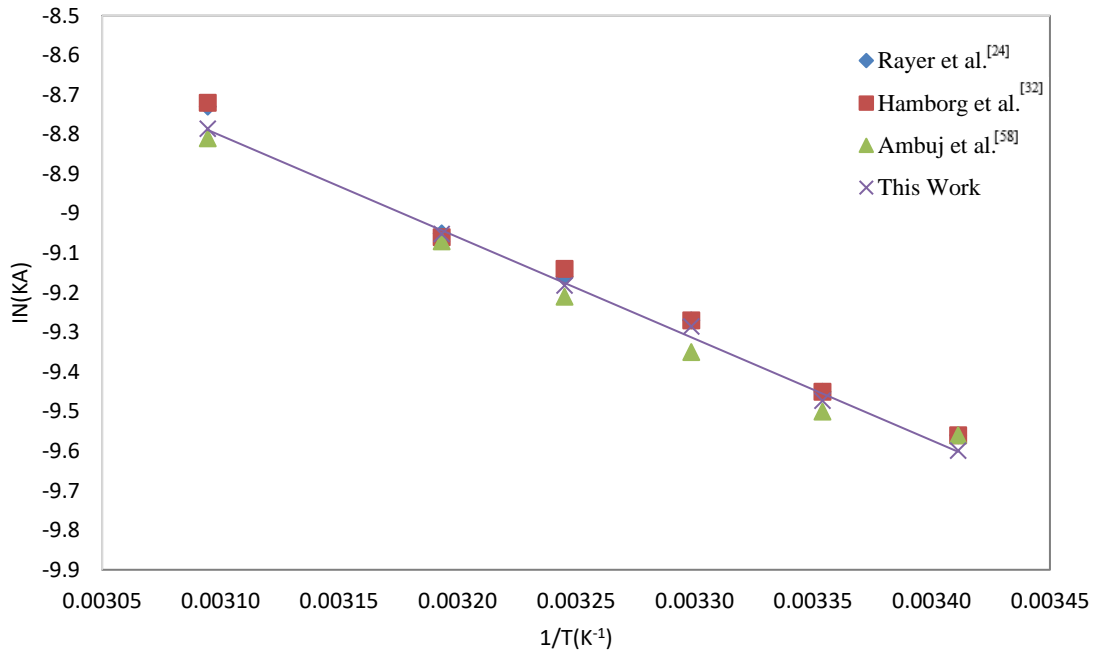


Figure 3.2 Comparative analysis of ionization constants of MEA between a specified range of temperatures of 298.15K and 313.15K.

Table 3.5 pK<sub>a1</sub> values of the studied amines at different temperatures

Chemical	pK <sub>a1</sub>					
	293.15K	298.15K	303.15K	308.15K	313.15K	323.15K
Monoethanolamine	9.60	9.47	9.29	9.18	9.05	8.79
3-(Diethylamino)propylamine	10.58	10.44	10.30	10.15	10.03	9.83
1,3-Diaminopentane	10.56	10.38	10.23	10.07	9.92	9.70
3-Butoxypropylamine	10.04	9.90	9.74	9.59	9.43	9.18
2-(Methylamino)ethanol	9.91	9.84	9.70	9.54	9.40	9.22
Bis(2-methoxyethyl)amine	8.69	8.62	8.51	8.37	8.25	8.07
$\alpha$ -Methylbenzylamine	9.50	9.37	9.17	8.94	8.83	8.57
2-Aminoheptane	10.71	10.53	10.24	9.99	9.24	8.65
3-Amino-1-phenylbutane	10.42	10.19	9.98	9.79	9.61	9.34

Table 3.6 pK<sub>a2</sub> values for the two diamines at different temperatures

Chemical	pK <sub>a2</sub>					
	293.15K	298.15K	303.15K	308.15K	313.15K	323.15K
3-(Diethylamino)propylamine	8.42	8.24	8.06	7.91	7.73	7.52
1,3-Diaminopentane	8.36	8.17	8.06	7.86	7.69	7.40

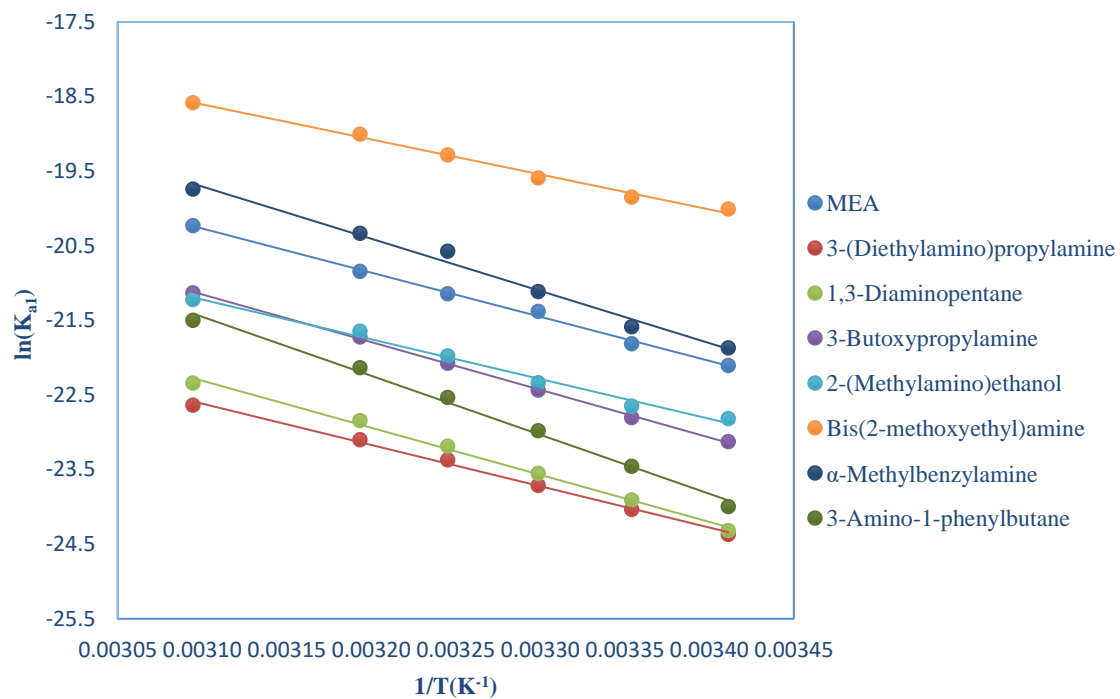
Based on the values obtained from the experimental data and calculations, we can observe that the amine basicity was susceptible to temperature because the pK<sub>a</sub> values decreased with an increase in temperature for the protonated amines.

The relationship between the ionization constant (K<sub>a</sub>), standard state enthalpy (ΔH<sup>0</sup>) and standard state entropy (ΔS<sup>0</sup>) are described in the van't Hoff equation (equation 3.9) [24].

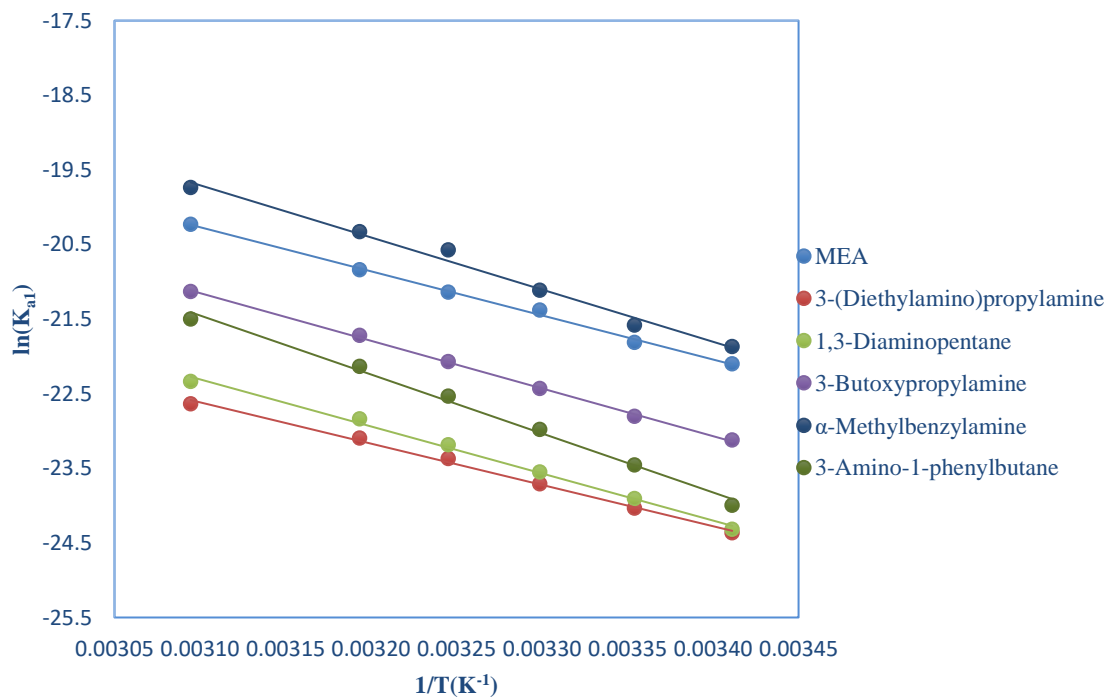
$$\ln(K_a) = -\frac{\Delta H^0}{RT} + \frac{\Delta S^0}{R} \quad \text{Eqn. 3.9}$$

Following the van't Hoff equation, there is a linear relation between ln(K<sub>a</sub>) and 1/T and the data was plotted in Figures 3.2, 3.3 and 3.4. The basicity of the amines was compared in Figures 3.3 and 3.4. As discussed earlier, pK<sub>a</sub> is the negative logarithm of K<sub>a</sub>, which means that ln(K<sub>a</sub>) value decreases as the amine's pK<sub>a</sub> value increases and vice versa. In Figure 3.3, the basicity of primary and secondary amines was compared. In Figure 3.4, the first and second dissociation constants were compared. The results for the calculated enthalpy and entropy values are listed in Tables 3.7 to 3.10.

(a)



(b)



(c)

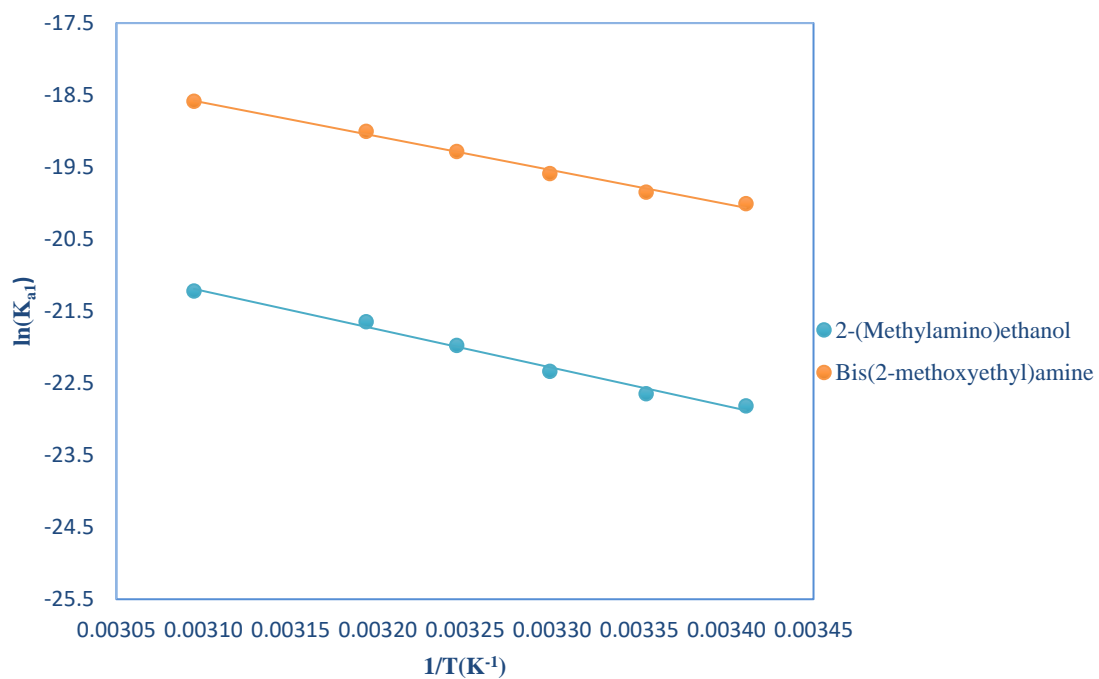
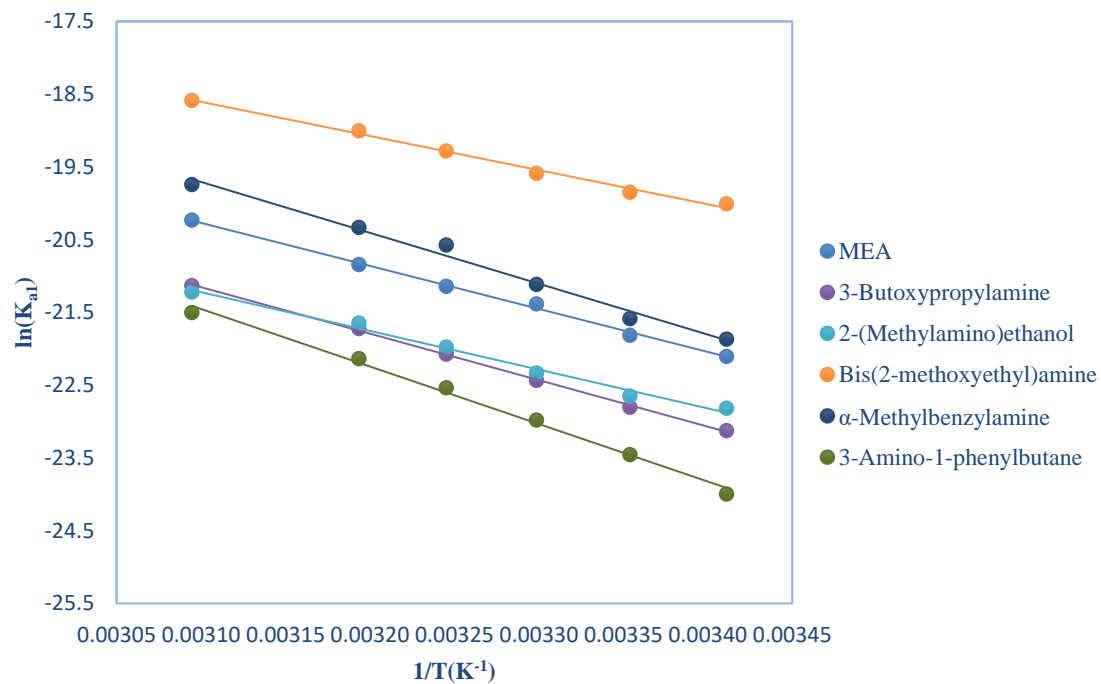


Figure 3.3  $\ln(K_{a1})$  vs  $1000/T$  f (a) all amines; (b) primary amines; and (c) secondary amine

(a)



(b)

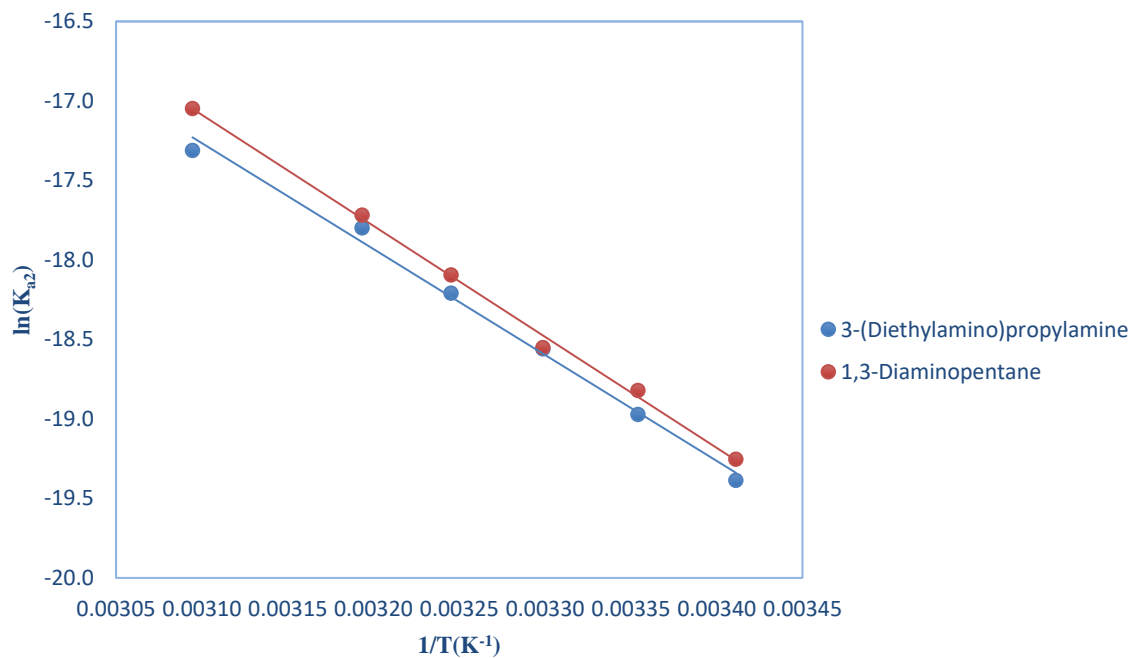


Figure 3.4  $\ln(K_a)$  vs  $1000/T$  for studied amines. (a)  $\ln(K_{a1})$  for monoamines (b)  $\ln(K_{a2})$  of diamines

Table 3.7 Standard state enthalpy change and entropy change of the first pK<sub>a</sub> of the studied amines

Solvent	$\Delta H^\circ$ (kJ·mol <sup>-1</sup> )	$\Delta S^\circ$ (kJ·mol <sup>-1</sup> ·K <sup>-1</sup> )
Monoethanolamine	49.16	-0.02
3-(Diethylamino)propylamine	46.03	-0.05
1,3-Diaminopentane	52.45	-0.02
3-Butoxypropylamine	53.14	-0.01
2-(Methylamino)ethanol	44.26	-0.04
Bis(2-methoxyethyl)amine	39.03	-0.03
$\alpha$ -Methylbenzylamine	58.14	0.02
2-Aminoheptane	130.72	0.24
3-Amino-1-phenylbutane	65.74	0.03

Table 3.8 Standard Gibbs-Free energy of reaction for the first pK<sub>a</sub> of the studied amines at various temperatures

$\Delta G^\circ$ (kJ·mol <sup>-1</sup> )						
Solvent	T (K)					
	293.15	298.15	303.15	308.15	313.15	323.15
Monoethanolamine	53.87	54.07	53.89	54.17	54.26	54.35
3-(Diethylamino)propylamine	59.39	59.58	59.76	59.88	60.14	60.82
1,3-Diaminopentane	59.27	59.26	59.36	59.40	59.47	60.02
3-Butoxypropylamine	56.36	56.53	56.54	56.55	56.55	56.78
2-(Methylamino)ethanol	55.61	56.14	56.29	56.30	56.36	57.01
Bis(2-methoxyethyl)amine	48.77	49.20	49.37	49.40	49.48	49.93
$\alpha$ -Methylbenzylamine	53.30	53.50	53.22	52.71	52.94	53.04
2-Aminoheptane	60.09	60.09	59.42	58.94	55.42	53.50
3-Amino-1-phenylbutane	58.49	58.14	57.92	57.73	57.63	57.76

Table 3.9 Standard state enthalpy change and entropy change of the second pK<sub>a</sub> of the studied amines

Solvent	$\Delta H^\circ$ (kJ·mol <sup>-1</sup> )	$\Delta S^\circ$ (kJ·mol <sup>-1</sup> ·K <sup>-1</sup> )
3-(Diethylamino)propylamine	55.36	0.03
1,3-Diaminopentane	58.06	0.04

Table 3.10 Standard Gibbs-Free energy of reaction for the second pK<sub>a</sub> of the studied amines at various temperatures

$\Delta G^\circ$ (kJ·mol <sup>-1</sup> )						
Solvent	T					
	293.15	298.15	303.15	308.15	313.15	323.15
3-(Diethylamino)propylamine	59.39	59.58	59.76	59.88	60.14	60.82
1,3-Diaminopentane	59.27	59.26	59.36	59.40	59.47	60.02

In the studied amines, it was observed that 2-Aminoheptane had the highest pK<sub>a</sub> value. Out of the 8 studied amines we had two diamines namely, 3-(Diethylamino) propylamine and 1,3-Diaminopentane, out of which 3-(Diethylamino) propylamine had a higher pK<sub>a</sub> value. As both are diamines, their second pK<sub>a</sub> values had to be further studied and based on the tabulated values it was observed that the diamine, 3-(Diethylamino) propylamine, is expected to be more reactive towards CO<sub>2</sub> than 1,3-Diaminopentane.

### 3.5 PDS prediction of $pK_a$ values for protonated amines

The main idea behind the Perrin–Dempsey–Serjeant (PDS) method was to predict  $pK_a$  values using a table with tabulated additive values of  $pK_a$  depending on the amino groups and corrections for functional groups [19]. This group additivity method is also called a computer-free method or paper and pencil method unlike other complex computational methods. In the PDS method,  $pK_a$  values can easily be predicted with acceptable accuracy. In some conditions, like in the case of the benzene effect, the deviations in prediction are comparatively higher.

In this prediction process, we have used three methods PDS, New PDS and the model proposed by Qian, Sun, Sun, and Gao, named QSSG. There have been two significant changes or updates to the PDS method which resulted in the new PDS method. This was achieved by updating the parameter values through least-square fits of new experimental  $pK_a$  data. [39]. The second significant modification was done by Qian et al. (QSSG), where the parameters were updated by taking additional factors like the steric hindrance, solvent and intramolecular hydrogen bonding into account. All these parameters are listed in Table 3.11 [40].

Table 3.11 pK<sub>a</sub> prediction using PDS, new PDS and QSSG methods [40].

Terms	Functional group	PDS values	New PDS values	QSSG values
Base value	Primary amine	10.77	10.60	10.60
	Secondary amine	11.15	11.10	10.80
	Tertiary amine	10.50	10.60	10.60
ΔpK <sub>a</sub> shifts	CH <sub>3</sub> on tertiary N	-0.2	-0.2	-0.2
	CH <sub>3</sub> on primary and secondary N	-0.2	-0.2	0
	β OR	-1.2	-1.4	-1.3
	β NH <sub>2</sub>	-0.8	-0.9	-0.9
	β NHR	-0.9	-1.0	-0.8
	β NR <sub>2</sub>	-0.9	-1.0	-1.0
	β OH	-1.1	-1.0	-1.0
	γ group	+0.4Δβ	+0.4Δβ	+0.6Δβ
	δ group	+0.4Δγ	+0.4Δγ	+0.6Δγ
	ε OH group	0	0	+0.6Δγ
	ring effect	+0.2	0	+0.2
	if two equivalent N sites	+0.3	+0.3	+0.3
	β- CH(CH <sub>3</sub> ) <sub>2</sub>	-	-	-0.3
β-C(CH <sub>3</sub> ) <sub>3</sub>			-0.45	

Terms	Functional group	PDS values	New PDS values	QSSG values
$\Delta pK_a$ shifts	solvent effects (CH <sub>2</sub> CH <sub>2</sub> OH) <sub>2</sub>			+0.3
	solvent effects (CH <sub>2</sub> CH <sub>2</sub> OH) <sub>3</sub>			+0.6
	steric effects of cyclic tertiary amine			-0.5
	intramolecular H bonding			+0.2

Table 3.12 pKa predictions using the PDS method

Chemical	Amine Type	Base Value	N-Me	$\beta$ -OR	$\beta$ -OH	$\gamma$ -group	$\delta$ -group	Ring Effect	PDS	Exp	error
Monoethanolamine	1	10.77	0	0	-1.1	0	0	0	9.67	9.47	0.2
3-(Diethylamino)propylamine	1	10.77	0	0	0	-0.36	0	0	10.41	10.43	-0.02
1,3-Diaminopentane	1	10.77	0	0	0	-0.32	0	0	10.45	10.39	0.06
3-Butoxypropylamine	1	10.77	0	0	0	0	-0.19	0	10.58	9.9	0.68
2-(Methylamino)ethanol	2	11.15	-0.2	0	0	-0.44	0	0	10.51	9.87	0.64
Bis(2-methoxyethyl)amine	2	11.15	0	2.4	0	0	0	0	8.75	8.64	0.11
$\alpha$ -Methylbenzylamine	1	10.77	0	0	0	0	0	0	10.77	9.37	1.4
2-Aminoheptane	1	10.77	0	0	0	0	0	0	10.77	10.52	0.25
3-Amino-1-phenylbutane	1	10.77	0	0	0	0	0	0.2	10.57	10.19	0.38
RMS											0.41

Table 3.13 pKa predictions Using the New PDS method

Chemical	Amine Type	Base Value	N-Me	$\beta$ -OR	$\beta$ -OH	$\gamma$ -group	$\delta$ -group	Ring Effect	PDS	Exp	error
Monoethanolamine	1	10.6	0	0	-1.0	0	0	0	9.60	9.47	0.13
3-(Diethylamino)propylamine	1	10.6	0	0	0	-0.40	0	0	10.20	10.43	-0.23
1,3-Diaminopentane	1	10.6	0	0	0	-0.36	0	0	10.24	10.39	-0.15
3-Butoxypropylamine	1	10.6	0	0	0	0	-0.22	0	10.38	9.9	0.48
2-(Methylamino)ethanol	2	11.1	-0.2	0	0.0	-0.40	0	0	10.50	9.87	0.63
Bis(2-methoxyethyl)amine	2	11.1	0	-2.8	0	0	0	0	8.30	8.64	-0.34
$\alpha$ -Methylbenzylamine	1	10.6	0	0	0	0	0	0	10.60	9.37	1.23
2-Aminoheptane	1	10.6	0	0	0	0	0	0	10.60	10.52	0.08
3-Amino-1-phenylbutane	1	10.6	0	0	0	0	0	0	10.60	10.19	0.41
RMS											0.25

Table 3.14 pKa predictions using the QSSG model

Chemical	Amine Type	Base Value	N-Me	$\beta$ -OR	$\beta$ -OH	$\gamma$ -group	$\delta$ -group	Ring Effect	PDS	Exp	error
Monoethanolamine	1	10.6	0	0	-1.0	0	0	0	9.60	9.47	0.13
3-(Diethylamino)propylamine	1	10.6	0	0	0	-0.48	0.00	0	10.12	10.43	-0.31
1,3-Diaminopentane	1	10.6	0	0	0	-0.36	0	0	10.24	10.39	-0.15
3-Butoxypropylamine	1	10.6	0	0	0	0	-0.47	0	10.13	9.9	0.23
2-(Methylamino)ethanol	2	10.8	0.2	0	0.0	-0.60	0	0	10.00	9.87	0.13
Bis(2-methoxyethyl)amine	2	10.8	0	2.6	0	0	0	0	8.20	8.64	-0.44
$\alpha$ -Methylbenzylamine	1	10.6	0	0	0	0	0	0	10.60	9.37	1.23
2-Aminoheptane	1	10.6	0	0	0	0	0	0	10.60	10.52	0.08
3-Amino-1-phenylbutane	1	10.6	0	0	0	0	0	0.2	10.80	10.19	0.61
RMS											0.17

The predicted  $pK_a$  values using PDS, new PDS and QSSG approaches are presented in Tables 3.12 to 3.14. We can observe that the root means square (RMS) error for the obtained results were 0.41, 0.25 and 0.17 respectively while comparing all three models, the RMS error was reduced from PDS to QSSG. We can observe that the error for  $\alpha$ -Methylbenzylamine was the highest when compared to other amines because of the benzene effect. The effect of the benzene ring will influence the reactivity of the compound in the prediction stage, and that compound's  $pK_a$  would be very hard to predict through the PDS method, as there are no specific parameters to predict that benzene effect.

## Chapter 4 : pK<sub>a</sub> Predictions of Amines using Artificial Neural Network (ANN)

### 4.1 Introduction

The experimental estimation of pK<sub>a</sub> values is usually a time-consuming process, hence an alternative approach of predicting the pK<sub>a</sub> values has been adopted. The interest to understand and learn more about the pK<sub>a</sub> values of un-synthesized compounds has seen a steady rise in the scientific community. The predictive approach helps with this purpose as well. Different strategies were adopted to improve the prediction accuracy using different approaches and algorithms. New and better predictive algorithms are being developed regularly. One such predictive tool is the Artificial Neural Network (ANN) and it has been explored in this work.

$$pK_a = \frac{\Delta G_{aq}}{RT \log 10} \quad \text{Eqn. 4.1}$$

The base of pK<sub>a</sub> is related to the energy change of a transferred proton in an aqueous solution the relation is given by equation 4.1 [41]. The major advantage of using an ANN model for prediction in comparison to the traditional PDS prediction of pK<sub>a</sub> is that the PDS provides a pK<sub>a</sub> value of a particular amine at 25° C, whereas the trained ANN model gives pK<sub>a</sub> value instantaneously over a range of temperatures. The model being developed spans at a temperature range of 293.15 K to 323.15 K. Another significant advantage of using an ANN model is its ability to predict the pK<sub>a</sub> of an amine having a benzene effect with an acceptable level of error which is not always possible in the case of PDS approach.

## 4.2 Background and Overview of ANN

ANN replicates the working of a human brain by using a different number of artificial neuron associations between each other. The basic ANN architecture is depicted in Figure 4.1 [42].

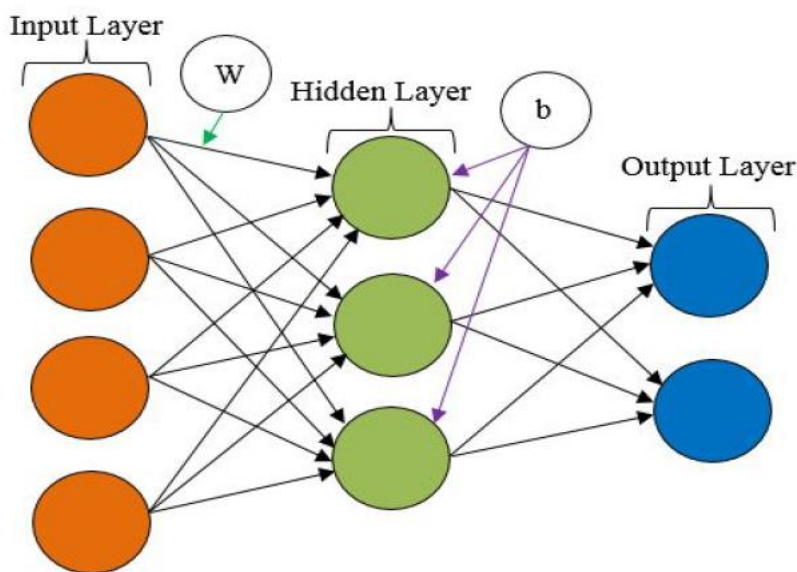


Figure 4.1 The basic ANN architecture

The major processing components of the ANN system are the neurons whose number is a deciding factor for the performance of the model. Sigmoid functions work on the inputs and weights and further help us to determine the output. The measure of connectivity of these weight values with the nodes is called a bias, which is calculated and assigned based on how the training data is linked and connected between layers. The network tends to identify particular traits of a cluster based on the traits portrayed by the input data, which in this case is a total number of 10 inputs. The total of two hidden layers with 40 and 39 neurons in each was designed with one output which is  $pK_a$  and is depicted in Figure 4.2.

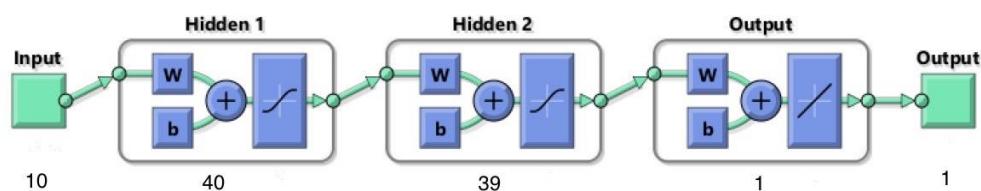


Figure 4.2 ANN architecture used in this work

#### 4.2.1 Feed-forward Neural Network

The Feed-forward network is among the most widely used ANN architecture for chemical engineering applications. In this model, the information flow is uni-directional right from the input layer to the output layer, irrespective of the number of hidden layers. The major issue with this model is that there is no feedback from one layer to another.

Functional transformations describe the functionality of an ANN model. The equations representing the same for a basic ANN model have been defined as the product of weights and the input signal with an addition of the bias vector further multiplied by the activation functions. The same has been outlined in the following Equation 4.2 [45]:

$$Y_i = P_i (W_i X_i + B_i) \quad \text{Eqn. 4.2}$$

Where  $P_i$  is the vector of activation functions,  $W_i$  is the weight from each neuron in each layer.  $X_i$  represents the input signal where  $i$  ranges from 1 to  $n$  and  $B_i$  represents the bias vector and  $Y_i$  is the total output of the particular layer.

An activation function is a function that is added to an ANN to help the network learn complex patterns of data. Generally, the output signal from one cell is fed to a function which is further converted into a form that can be taken as an input to the next cell. Without the activation

function, the network would be rendered as a simple linear regression model that greatly restricts the ability of the model to solve complex cases.

We need to consider a non-linear activation function to limit the complexity of the function as it is a product of weights and input added to the bias. For instance, if we have a huge neural network, we may end up with a value of a very high magnitude. There are various types of non-linear activation functions like Sigmoid, Softmax, Tanh, ReLU, etc [45]. The most popular and fairly complex activation function among these is the Sigmoid function which has been used in this study. The function is presented in Equation 4.3 [45]

$$S(x) = \frac{1}{1 + e^{-x}} \quad \text{Eqn. 4.3}$$

#### 4.2.2 Backpropagation algorithm

Backpropagation in the neural network is an alternative name for the backward propagation of errors. With the weights in the network, the gradient of the loss function is calculated. The weights can be fine-tuned based on the error rate obtained in the previous epoch (iteration) which would help reduce the error rates and further makes the model more reliable.

In the considered ANN architecture depicted in Figure 4.2, the input arrived through the preconnected path and the inputs were modelled using real weights which were selected randomly. The output was computed for each neuron that moved between the input and output layer passing through any number of hidden layers. The difference between the actual output and the desired output would give us the error observed in the output. Finally, we moved back to the hidden layer from the output layer to adjust the weights to decrease the error. This entire process was recursively repeated until we reached the desired output value. This entire work process can be described with the following equations 4.4 to 4.7 [23]:

In the case of the hidden layer:

$$net_q = \sum_{i=0}^{N^{input}} V_{ji} X_i \quad \text{Eqn. 4.4}$$

$$H_j = \sigma(net_q) \quad \text{Eqn. 4.5}$$

In the case of the output layer:

$$net_z = \sum_{j=0}^{N^{hidden}} W_{jk} H_j \quad \text{Eqn. 4.6}$$

$$O_k = \sigma(net_z) \quad \text{Eqn. 4.7}$$

For the  $i^{\text{th}}$  neuron in the input layer,  $X_i$  was the output;  $V_{ji}$  represented the weight generated by the connection between the  $i^{\text{th}}$  in input and  $j^{\text{th}}$  neuron present in the hidden layer;  $N^{input}$  gave the upper range of the number of neurons in the input layer of the model;  $net_q$  generated the output from the first layer and fed it in as the input to the  $j^{\text{th}}$  neuron present in the hidden layer; the activation function was given by  $\sigma$  which in our case was the sigmoid equation;  $H_j$  gave the overall output of the  $j^{\text{th}}$  neuron coming from the hidden layer;  $W_{jk}$  gave the weight associated between the  $j^{\text{th}}$  neuron in the hidden layer to the  $k^{\text{th}}$  neuron in the output layer;

In the hidden layer,  $N^{hidden}$  gave the number of neurons;  $net_z$  represented the overall input to the  $k^{\text{th}}$  neuron associated with the output layer, and  $O_k$  gave the final output of the  $k^{\text{th}}$  neuron.

The general equations used to calculate necessary weight changes based on the target data and input data are given by Equations 4.8 and 4.9 [23]:

$$W_{jk}(new) = W_{jk}(old) + \Delta W_{jk} \quad \text{Eqn. 4.8}$$

$$V_{ji}(new) = V_{ji}(old) + \Delta V_{ji} \quad \text{Eqn. 4.9}$$

The necessary weight changes were computed by the  $\Delta$  function in the above equations. The change in weights is defined as the product of error function and a partial derivative constant and the neurons from the hidden layer. The first equation represented the change of weights between the hidden layer and the input layer and the second equation represented the change in weights between the output layer and the hidden layer. The error function  $\delta$  made the backpropagation possible and ensured that a connection between neurons of one layer and its previous layer was maintained. We repeated the process of correcting weights and increased the number of hidden layers until we reached a minimal error as desired.

### 4.3 Data aggregation and variable selection

The major challenge in variable selection and data aggregation was converting the structural information of pK<sub>a</sub> values into numerical values that can be fed into the ANN model that has been devised. The other major challenge was to handle different temperatures in the process of pK<sub>a</sub> prediction. The majority of the generic data was limited to a single temperature of either 20 or 25 °C, whereas the experimental data measured in this work involved 5 different temperatures. This was the major reason why we needed to develop a flexible model that would accurately predict the pK<sub>a</sub> values of the amines at varying temperatures. The objective was to enable the prediction of pK<sub>a</sub> for the physical properties of the compound referring to ANN inputs.

Collecting a diverse range of data to feed as input into the ANN model was a laborious task. A significant amount of data was collected from different literature sources as outlined in Table

4.1 This data was enhanced by adding the experimental data recorded in this work for pK<sub>a</sub> prediction. In total, 677 data points relevant to CO<sub>2</sub> capture were used as inputs to the model being trained. The data can be segregated widely into three segments, 1) The properties that were used to identify the compound which was considered as the inputs (Temperature, Molecular Weight, Number of H atoms, N atoms, C atoms and O atoms). 2) The properties that were used to correlate the pK<sub>a</sub> values (Density, Viscosity, Refractive Index and Sound Velocity). 3) The experimentally determined pK<sub>a</sub> values which was the output.

Table 4.1 Data aggregation used in this work

Amines	CAS Number	Temperature(K)	Data Points	Reference
Methyldiethanolamine (MDEA)	105-59-9	298.15 – 313.15	32	[51,0]
1-amino-2-propanol (MIPA)	78-96-6	298.15 – 313.15	24	[43,57]
Dimethylpropanolamine (DMPA)	3179-63-3	298.15 – 313.15	24	[26,58]
2-(Methylamino)ethanol (MAE)	109-83-1	298.15 – 313.15	24	[55,56]
2-amino-2-methyl-1-propanol(AMP)	124-68-5	298.15 – 313.15	24	[56,59-62]
Diethanolamine (DEA)	111-42-2	298.15 – 313.15	32	[53,63-66]
Triethanolamine (TEA)	102-71-6	298.15 – 313.15	24	[16,31-33,35-39]
3-amino-1-propanol (3AP)	105-87-6	298.15 – 313.15	24	[43,67,68]
N,N-Dimethylethanolamine (DMEA)	108-01-0	298.15 – 308.15	16	[34,69-74]
Ethyldiethanolamine (EDEA)	139-87-7	298.15	8	[26,67]
2-(Ethylamino)ethanol (EMEA)	110-73-6	298.15	8	[33,70,0]
Diethylethanolamine (DEEA)	100-37-8	298.15	8	[33,55,76]
Butylamine (BA)	109-73-9	298.15	8	[77-80]

Tert-butylamine (tert-BA)	75-64-9	298.15	8	[44-46]
3-(Dimethylamino)-1-Propylamine (DMAPA)	109-55-7	298.15	8	[58,80,81]
N-(2-Aminoethyl)-1,3-propanediamine (n-2AOE13PDA)	13531-52-7	298.15 – 313.15	28	[23]
Bis[2-(N,N-dimethylamino)ethyl] ether (2DMAOEE)	3033-62-3	298.15 – 313.15	28	[23]
N,N-Dimethyldipropylenetriamine (DMAPAPA)	10563-29-8	298.15 – 313.15	28	[23]
3,3'-Diamino-N-methyldipropylamine (DAOMDPA)	105-83-9	298.15 – 313.15	28	[23]
2-[2-(Dimethylamino)ethoxy]ethanol (DMAOEOE)	1704-62-7	298.15 – 313.15	28	[23]
2-(Dibutylamino)ethanol (DBEA)	102-81-8	298.15 – 313.15	28	[23]
N-Propylethanolamine (PEA)	16369-21-4	298.15 – 313.15	28	[23]
Monoethanolamine	141-43-5	298.15 – 323.15	45	This work*
3-(Diethylamino)propylamine	104-78-9	298.15 – 323.15	45	
1,3-Diaminopentane	589-37-7	298.15 – 323.15	45	
3-Butoxypropylamine	16499-88-0	298.15 – 323.15	45	
2-(Methylamino)ethanol	109-83-1	298.15 – 323.15	45	
Bis(2-methoxyethyl)amine	111-95-5	298.15 – 323.15	45	
$\alpha$ -Methylbenzylamine	618-36-0	298.15 – 323.15	45	
2-Aminoheptane	123-82-0	298.15 – 323.15	45	
3-Amino-1-phenylbutane	22374-89-6	298.15 – 323.15	45	

\* The data extraction process has been outlined in detail in Appendix A

## 4.4 ANN Model and Observations

### 4.4.1 Model with all recorded input parameters

A total of 10 input parameters were introduced to the model including the molecular weight, the number of atoms (H, C, N, O) that were used to identify the compounds. The temperature, density, viscosity, refractive index and sound velocity were used as variables for modelling.

In the process of modelling, the dataset was divided into 3 sections for training, validation and testing. Data representing 70% of the entire database was randomly chosen as the training set 15% of the remaining data was chosen for validation and the final 15% was used for testing the resultant network with the unseen data.

Any model or network gave its best performance when we optimized and fine-tuned the workflow. The major optimizations that were adopted in this work included choosing the appropriate number of hidden layers, choosing the number of optimal neurons in each hidden layer and choosing the number of epochs that gave us a model with minimal MSE.

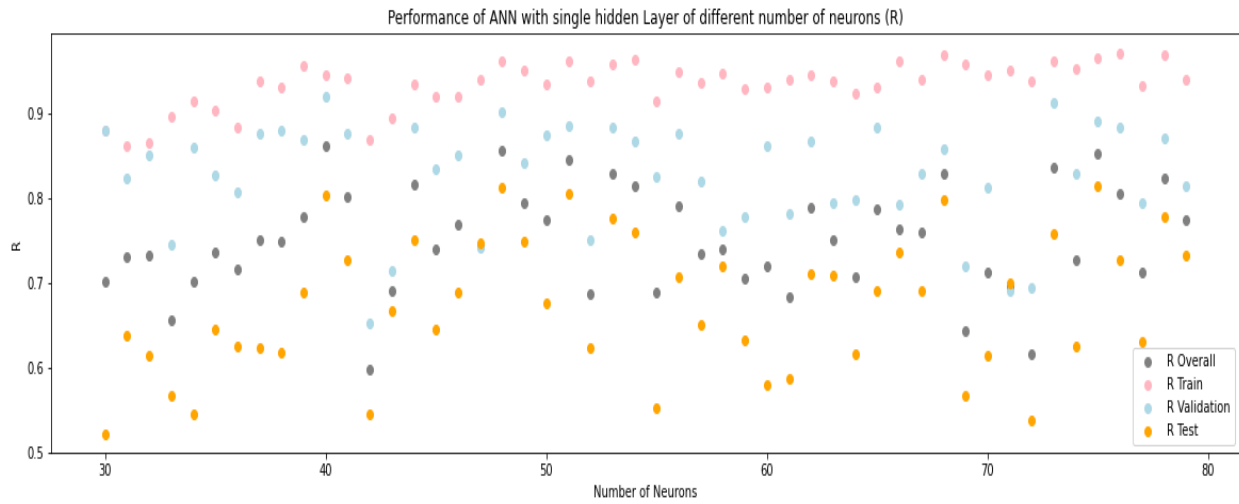
Ideally, we do not have a formulated method to decide the number of hidden layers or the number of neurons in each hidden layer. Hence, the program was modelled initially with one hidden layer and the number of neurons was kept a variable and run over the range of 30 to 80 and the R and MSE values were recorded and graphically represented.

Figure 4.3 outlined the model's performance considering a varying number of neurons in the first hidden layer with 10 inputs. The values compared were the R and mean squared error (MSE). We can observe that the model performed comparatively well when there were 40 neurons in the first hidden layer ( $R_{\text{overall}} = 0.86156$ ,  $MSE_{\text{train}} = 0.0288$ ,  $MSE_{\text{validation}} = 0.0460$  and  $MSE_{\text{test}} = 0.09044$ ). For now, we have an architecture that can be described as 10-40-1. To

check if the addition of a new hidden layer would improve the performance of the model, the first hidden layer was fixed with 40 neurons and the second hidden layer was executed with a variable range of 10 to 50 neurons. Figure 4.4 outlines the model's performance considering the varying number of neurons in the second hidden layer. We can observe that there was a significant improvement in the overall performance of the model by the introduction of the second layer at the mark when it had 39 neurons ( $R_{\text{overall}} = 0.9075$ ,  $MSE_{\text{train}} = 0.0069$ ,  $MSE_{\text{validation}} = 0.0372$  and  $MSE_{\text{test}} = 0.0597$ ). The addition of a third hidden layer was tried as well but it did not improve the overall model by a significant number. Hence 10-40-39-1 was chosen as the best ANN architecture. The weights and bias values for the second hidden layer generated by the ANN network are of a dimension 40\*39, hence it has been attached as a reference in Appendix B.

Overfitting of a model occurs when the designed ANN model would be able to predict the output with high accuracy for data that has been included in the training set and is not good at classifying the data in the validation and testing data set. To avoid overfitting in our model it was ensured that the right balance between the variables and hyper parameters were chosen including the epochs, number of neurons and also the batch size.

(i)



(ii)

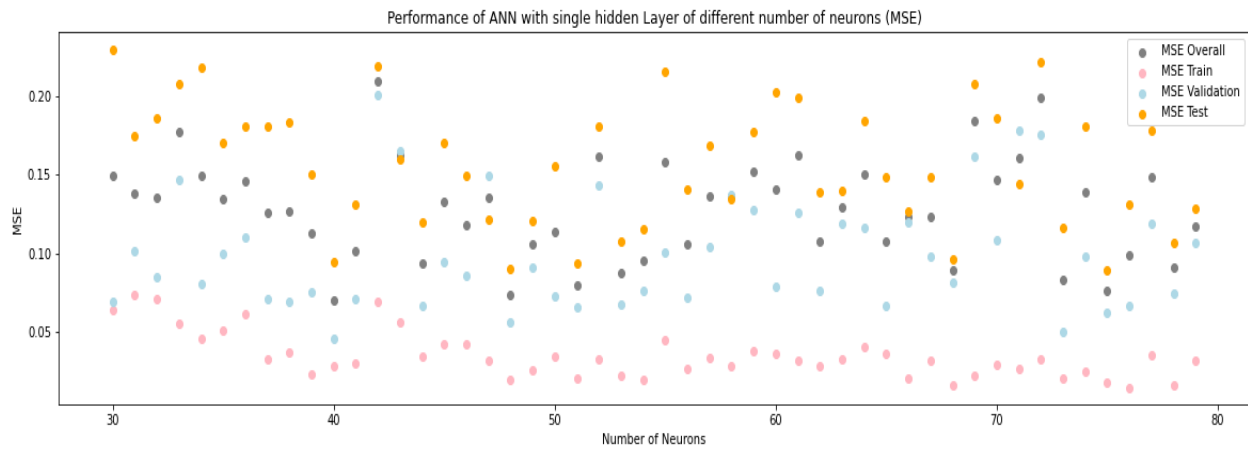
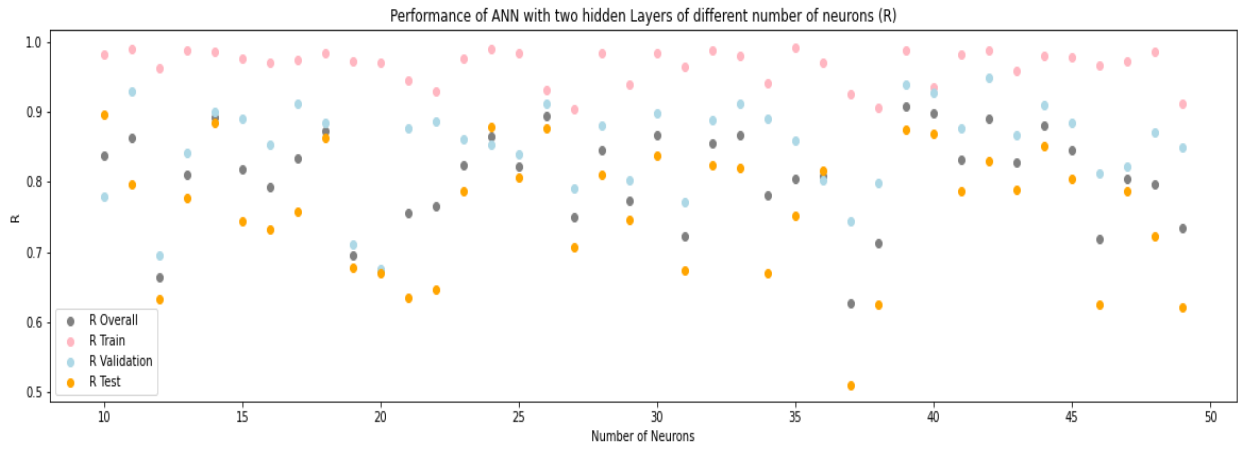


Figure 4.3 ANN performance with respect to varying number of neurons in the first hidden layer. (i) R; (ii) MSE.

(i)



(ii)



Figure 4.4 ANN performance with respect to varying number of neurons in the second hidden layer. (i) R; (ii) MSE.

The final proposed architecture is described in Figure 4.5. The final tuning step involved determining the best overall performance by running a varying number of epoch values ranging between 140 to 200 as depicted in Figure 4.6. It can be observed that the best performance with respect to overall MSE was observed at epoch 166 with a value of 0.026.

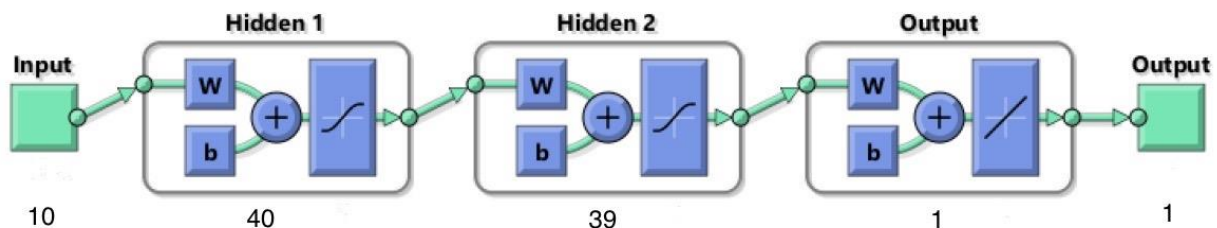


Figure 4.5 Final ANN architecture for pK<sub>a</sub> prediction.

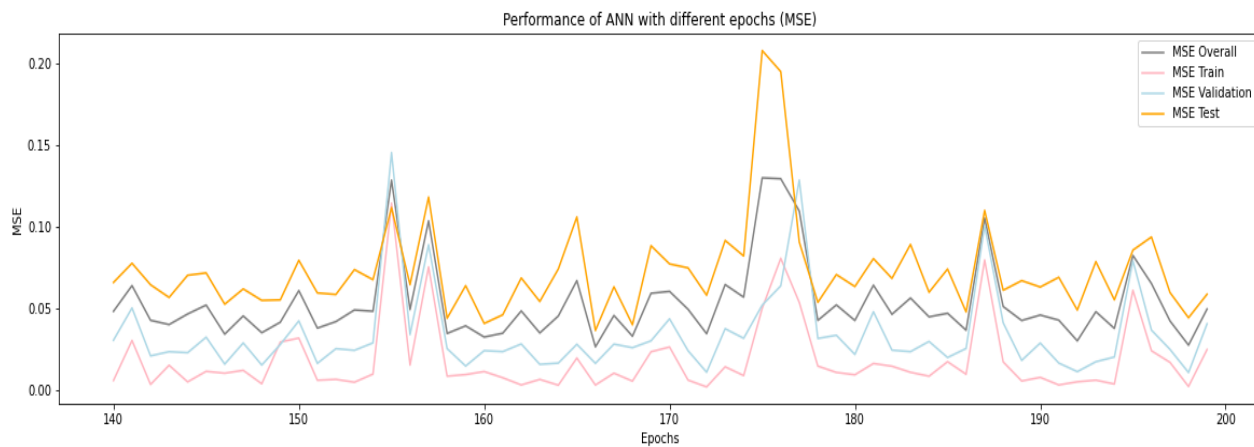


Figure 4.6 Performance of ANN with different epochs (MSE)

The following Figure 4.7 represents a comparative plot between output and target for the entire dataset including training, validation and testing. It can be found that  $R_{\text{overall}}$  was above 0.90, and hence has a very good predictive accuracy of  $\text{pK}_a$  values and a low MSE was obtained.

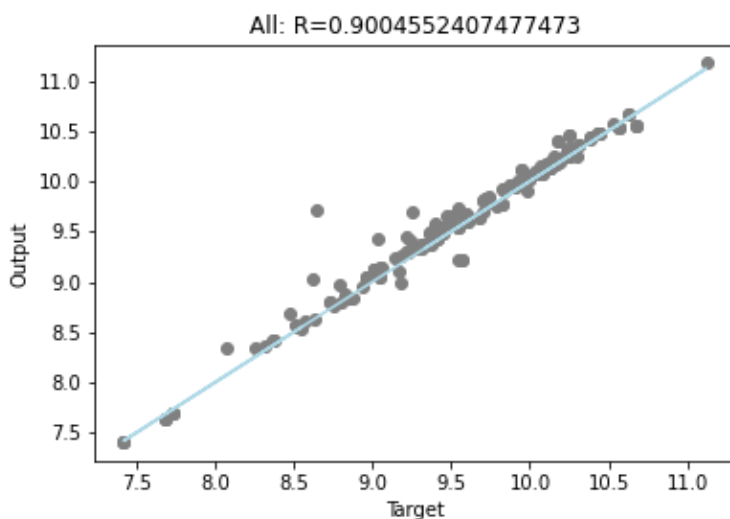


Figure 4.7 Scatter plot for the regressive prediction of  $\text{pK}_a$

The error histogram is depicted in Figure 4.8, which shows that there are only a few outliers. It can be observed that the majority of the errors are close to -0.06303, which is also close to the zero line.

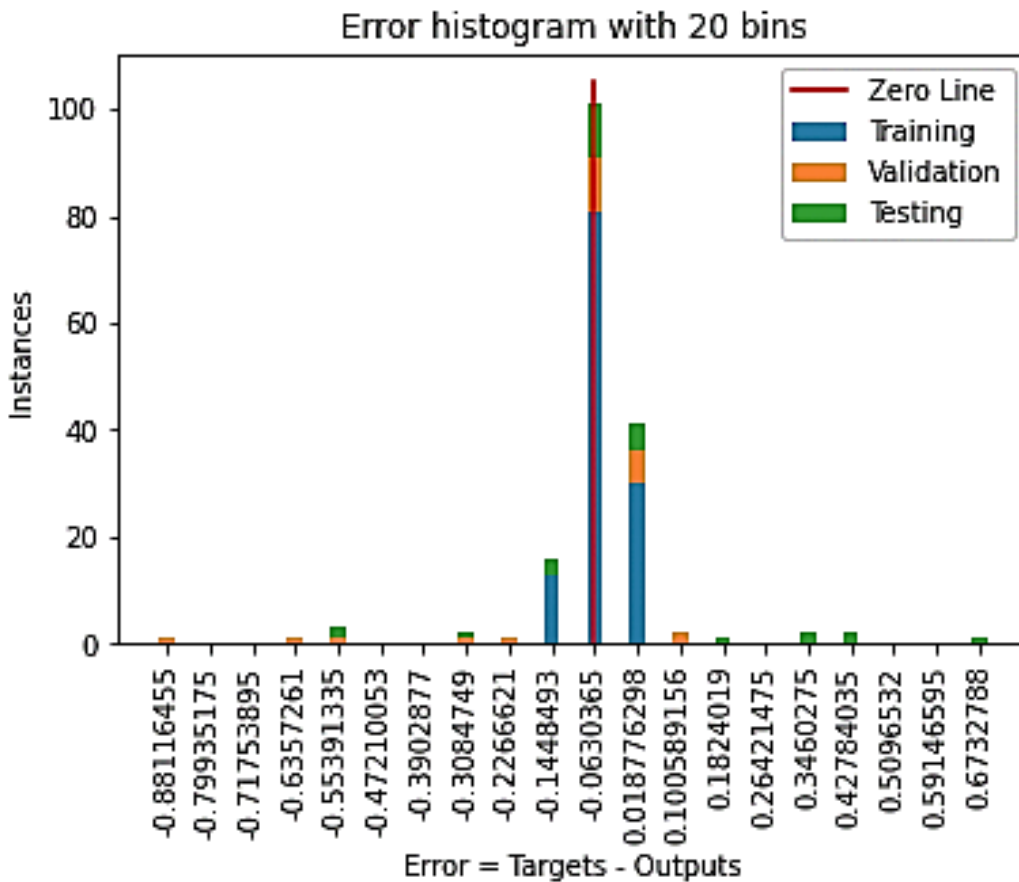


Figure 4.8 Zero-line representation in an error histogram

#### 4.4.2 Model with optimized input parameters

An ANN model with good prediction accuracy was obtained as outlined in section 4.4.1. However, to make the model more robust and faster, further investigation was performed on the input parameters and it was concluded that a model with a lesser number of input parameters would be beneficial in terms of speed and also helped in cases where the dataset is limited and estimation of a few input parameters were difficult. The temperature was kept unchanged as an input parameter due to its direct relation to the change in  $pK_a$  values. This section further explored the omission of several input parameters to have an acceptable trade-off between complexity and speed.

Extensive combinations of optimization were applied and it was found that the model was performing worst in every scenario except after removing the refractive index and sound velocity as input parameters. The  $R_{\text{overall}}$  was observed to be 0.89225 and the MSE values were  $\text{MSE}_{\text{train}} = 0.00881$ ,  $\text{MSE}_{\text{validation}} = 0.02945$  and  $\text{MSE}_{\text{test}} = 0.0798$  which provided good prediction results as well. All the combinations that were tested are reported in Table 4.2.

Table 4.2 Comparison of different ANN models' performance

Inputs Removed	$R_{\text{overall}}$	$\text{MSE}_{\text{train}}$	$\text{MSE}_{\text{validation}}$	$\text{MSE}_{\text{test}}$
Density	0.8165	0.0139	0.1127	0.0882
Refractive Index	0.8295	0.002	0.6125	0.1453
Sound Velocity	0.8425	0.01272	0.1369	0.0369
Viscosity	0.6939	0.05784	0.1931	0.1629
Molecular Weight	0.79761	0.03166	0.09731	0.11316
Sound Velocity & MW	0.8416	0.0053	0.0740	0.0903
Refractive Index & MW	0.8321	0.0084	0.0847	0.0905
Density & MW	0.7231	0.0058	0.1476	0.1427
Density & Sound Velocity	0.8871	0.01051	0.06614	0.05324
Density & Refractive Index	0.6270	0.03673	0.24193	0.15626
Density & Viscosity	0.8141	0.00382	0.12018	0.07821
Refractive Index & Sound Velocity	0.8922	0.00881	0.02945	0.0789
Refractive Index & Viscosity	0.6970	0.00279	0.11456	0.19534
Sound Velocity & Viscosity	0.7965	0.00798	0.10864	0.10478

The new ANN model that was obtained performed slightly weaker compared to the model outlined in section 4.4.1. On further analysis of the newly optimized model, it was observed that the  $pK_a$  predictions were in line with the actual outputs. Figure 4.9 shows that the number of epochs that provided the best output was 187.

In Figures 4.10 and 4.11, it is observed that the total number of outliers was low and the data was in close agreement with the zero line with an average value of 0.0136. The weights and biases are reported in Appendix B.

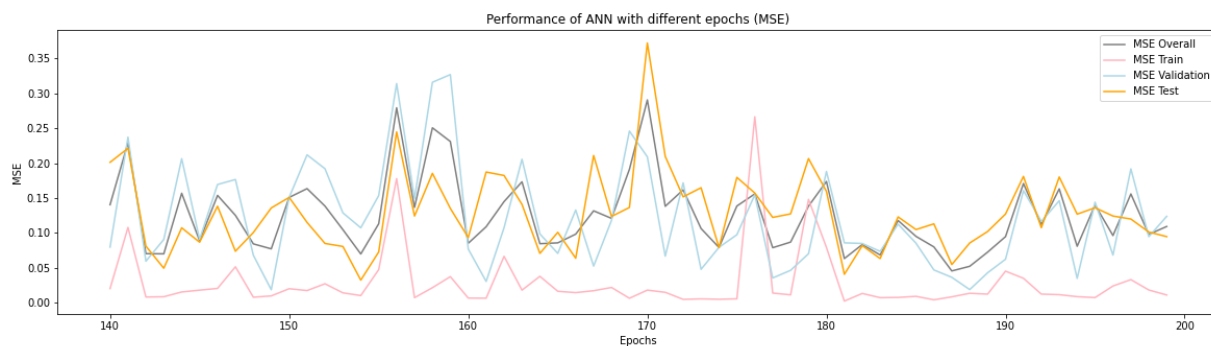


Figure 4.9 Enhanced performance of the model with respect to the optimized input parameters.

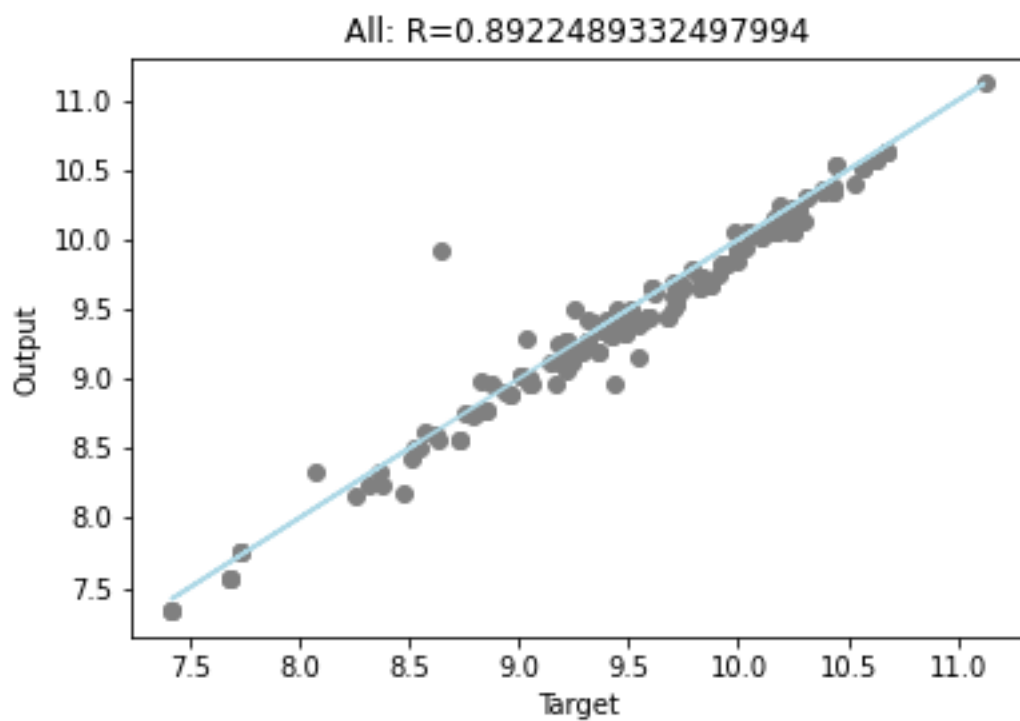


Figure 4.10 Scatter plot for the regressive prediction of pKa for the new model

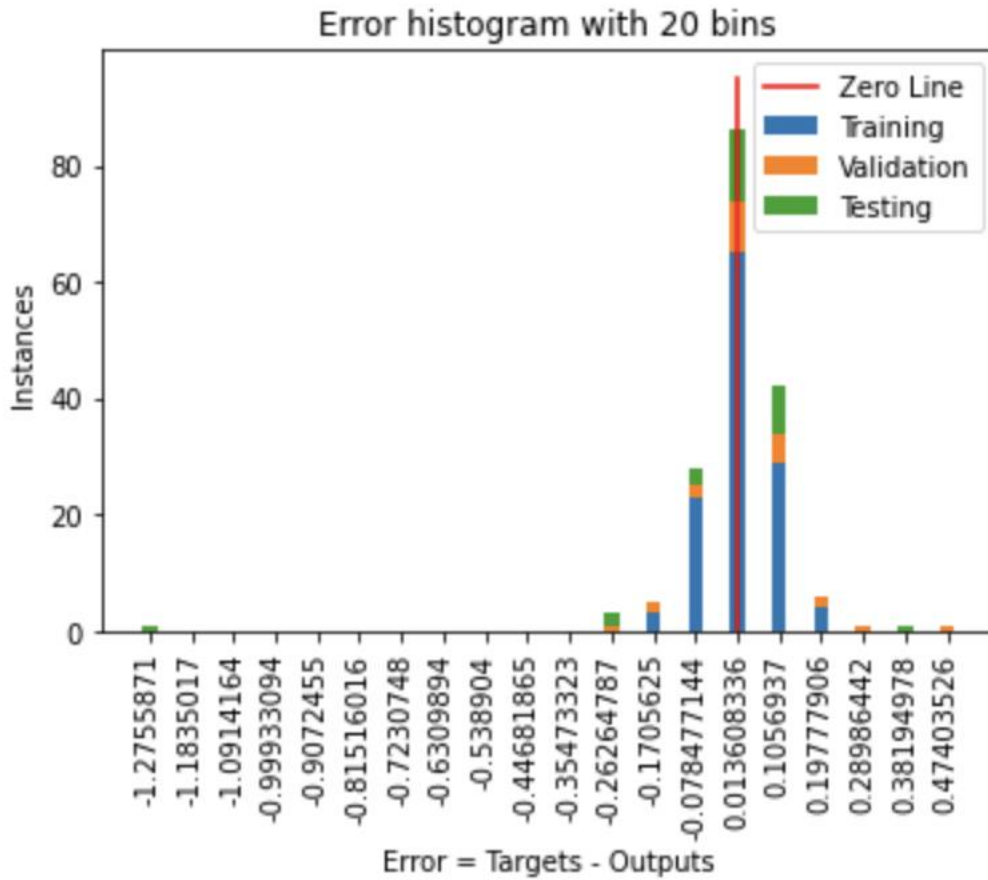


Figure 4.11 Error histogram of the optimized ANN model

The prediction accuracy was observed to be very close to the actual value. It can be noted that a standard deviation of 0.02 was observed in the best case and a standard deviation of close to 0.5 was observed in the worst-case scenario. A few example predictions are presented in Figures 4.12 to 4.14.

```
Enter your choice: 1
>>> Temperature: 25
>>> Molecular weight: 87.16
>>> number of Carbons: 5
>>> number of Hydrogen: 13
>>> number of Nitrogen: 1
>>> number of Oxygen: 0
>>> density: 0.751
>>> viscosity: 0.52
The pKa value is: 10.717925
Continue? Press 1
Exit? Press 2
```

Figure 4.12 pKa prediction for amine 1.

```
>>> Temperature: 25
>>> Molecular weight: 105.14
>>> number of Carbons: 4
>>> number of Hydrogen: 11
>>> number of Nitrogen: 1
>>> number of Oxygen: 2
>>> density: 1.0940
>>> viscosity: 566.3
The pKa value is: 8.9571295
Continue? Press 1
```

Figure 4.13 pKa prediction for amine 2.

```
>>> Temperature: 30
>>> Molecular weight: 89.14
>>> number of Carbons: 4
>>> number of Hydrogen: 11
>>> number of Nitrogen: 1
>>> number of Oxygen: 1
>>> density: 1.0907
>>> viscosity: 383.9
The pKa value is: 8.822975
Continue? Press 1
Exit? Press 2
```

Figure 4.14 pK<sub>a</sub> prediction for amine 3.

## Chapter 5 : Conclusion

pK<sub>a</sub> values of eight amines, namely, 3-(Diethylamino) propylamine, 1,3-Diaminopentane, 3-Butoxypropylamine, 2-(Methylamino) ethanol, Bis(2-methoxyethyl) amine,  $\alpha$ -Methylbenzyl amine, 2-aminoheptane, and 3-Amino-1-phenylbutane were experimentally measured at six different temperatures in the range of 298.15K to 323.15K using the potentiometric titration method.

It was observed that as the temperature increased the basicity of amines decreased. 2-Aminoheptane, a primary amine, and the two diamines studied, 3-(Diethylamino)propylamine with a primary and a tertiary amine, and 1,3-Diaminopentane with two primary amines had the highest pK<sub>a</sub>s of all eight amines. pK<sub>a</sub> values were predicted for the eight amines using the Perrin–Dempsey–Serjeant (PDS), the new PDS and the Qian, Sun, Sun, and Gao (QSSG) models. van't Hoff equation was utilized to determine thermodynamic properties such as the standard state enthalpy change ( $\Delta H^0$ ) and the standard state entropy change ( $\Delta S^0$ ) for the dissociation process.

pK<sub>a</sub> values of a set of amines of importance in the process of CO<sub>2</sub> capture were predicted using an Artificial Neural Network (ANN) with a backpropagation algorithm. Additionally, properties like the density, viscosity, refractive index and sound velocity of the selected eight amines were measured experimentally at the range of temperatures from 298.15 to 323.18 K.

Ten parameters were used as input data in this estimation in 2 subcategories. The first included the molecular weight, numbers of H, N, C and O atoms. The second included the temperature, density, viscosity, refractive index, and sound velocity. An architecture with a structure of 10-40-39-1 was selected as the desired ANN model and a prediction user interface was also developed. The predicted values were in close agreement with the experimental values.

The optimized architecture was a structure of 8-40-39-1. This model had a regression coefficient of 0.89225 and MSE values of 0.00881, 0.02945 and 0.0789 for the training, validation and testing datasets, respectively.

## References

1. Rayer, A.V.R. (2012). Screening of solvents for CO<sub>2</sub> capture: Kinetics, solubility and calorimetric studies (Doctoral dissertation, University of Regina).
2. Friedlingstein, P., Jones, M. W., O'Sullivan, M., Andrew, R. M., Bakker, D. C., Hauck, J., ... & Zeng, J. (2021). Global Carbon Budget 2021. *Earth System Science Data Discussions*, 1-191.
3. International Energy Agency. CO<sub>2</sub> Emissions from Fuel Combustion 2012. Paris: Organisation for Economic Co-operation and Development, 2012.
4. International Transport Forum. Reducing Transport Greenhouse Gas Emissions: Trends & Data. Paris: Organisation for Economic Co-operation and Development, 2010.
5. Koysoumpa, E.I., Bergins, C., & Kakaras, E. (2017). The CO<sub>2</sub> economy: Review of CO<sub>2</sub> capture and reuse technologies. *The Journal of Supercritical Fluids*, 132, 3-16.
6. Al-Mamoori, A., Krishnamurthy, A., Rownaghi, A. A., & Razeai, F. (2017). Carbon capture and utilization update. *Energy Technology*, 5, 834-849.
7. Ang, B., & Su, B. (2016). Carbon emission intensity in electricity production: A global analysis. *Energy Policy*, 56-63.
8. Koysoumpa, E.I., Bergins, C., & Kakaras, E. (2017). The CO<sub>2</sub> economy: Review of CO<sub>2</sub> capture and reuse technologies. *The Journal of Supercritical Fluids*, 132, 3-16.
9. Field, C.B., & Vicente, R. (2014). Climate change 2014: Impacts, adaptation, and vulnerability. Part A: Global and sectoral aspects. Cambridge: Cambridge University Press.
10. Page, B., Turan, G., Zapantis, A., Burrows, J., Consoli, C., Erikson, J., ... & Zhang, T. (2020). The Global Status of CCS 2020: Vital to Achieve Net Zero.
11. Creamer A.E., Gao B. (2015) Overview of CO<sub>2</sub> Capture Technology. In: Carbon Dioxide Capture: An Effective Way to Combat Global Warming. Springer Briefs in Molecular Science. Springer, Cham. [https://doi.org/10.1007/978-3-319-17010-7\\_2](https://doi.org/10.1007/978-3-319-17010-7_2).
12. Astaria, G., Savage, D.W., & Bisio, A. (1983) Gas treating with chemical solvents. New York, NY: John Wiley & Sons.
13. Leung, D.Y., Caramanna, G., & Maroto-Valer, M.M. (2014). An overview of current status of carbon dioxide capture and storage technologies. *Renewable and Sustainable Energy Reviews*, 39, 426-443.

14. Maginn, E.J. (2010). What to do with CO<sub>2</sub>? *Journal of Physical Chemistry Letters*, 1(24), 3478-3479.
15. Christensen, K., & Stupin, W. (1978). Merits of acid-gas removal processes. *Hydrocarbon Processing*, 57, 125-130.
16. Tennyson, R., & Schaaf, R. (1977). Guidelines can help choose proper process for gas-treating plants. *Oil Gas Journal*, 75(2), 78.
17. Kim, I., Hoff, K.A., Hessen, E. T., Haug-Warberg, T., & Svendsen, H. F. (2009). Enthalpy of absorption of CO<sub>2</sub> with alkanolamine solutions predicted from reaction equilibrium constants. *Chemical Engineering Science*, 64(9), 2027-2038.
18. Albert, A. (2012). *The determination of ionization constants: A laboratory manual*. New York, NY: Springer Science & Business Media.
19. Perrin, D.D., Dempsey, B., & Serjeant, E.P. (1981). *pK<sub>a</sub> prediction for organic acids and bases (Vol. 1)*. New York, NY: Chapman and Hall.
20. Qiang, Z., & Adams, C. (2004). Potentiometric determination of acid dissociation constants (pK<sub>a</sub>) for human and veterinary antibiotics. *Water Research*, 38(12), 2874-2890.
21. Nath, D., & Henni, A. (2020). Solubility of carbon dioxide (CO<sub>2</sub>) in aqueous solution of 3-(dimethylamino)-1-propylamine (DMAPA). *Fluid Phase Equilibria*, 511, 112506.
22. Joback, K. G., Heberle, J. R., & Bhowan, A. S. (2017). Influence of pK<sub>a</sub> and amine structure on energy consumption of post-combustion CO<sub>2</sub> capture processes. *Energy Procedia*, 114, 1689-1708.
23. Liu, G. (2018). *Experimental and Prediction Approaches to Determine Dissociation Constants (pK<sub>a</sub>) of Amines (Master's dissertation, University of Regina)*.
24. Nguyen, W. H. C. H., & Henni, A. (2020). Dissociation Constant (p K a) and Thermodynamic Properties of 1, 4-Bis (3-aminopropyl) Piperazine, 1, 3-Bis (aminomethyl) Cyclohexane, Tris (2-aminoethyl) Amine, and 1-Amino-4-methyl Piperazine: Study of the Protonation Mechanism Using the Density Function Theory. *Journal of Chemical & Engineering Data*, 65(5), 2280-2290.
25. Yu, C. H., Huang, C. H., & Tan, C. S. (2012). A review of CO<sub>2</sub> capture by absorption and adsorption. *Aerosol Air Qual. Res*, 12(5), 745-769.
26. Rayer, A.V., Sumon, K. Z., Jaffari, L., & Henni, A. (2014). Dissociation constants(pK<sub>a</sub>) of tertiary and cyclic amines: Structural and temperature dependences. *Journal of Chemical & Engineering Data*, 59(11), 3805-3813.

27. Tagiuri, A., Mohamedali, M., & Henni, A. (2015). Dissociation constant ( $pK_a$ ) and thermodynamic properties of some tertiary and cyclic amines from (298 to 333) K. *Journal of Chemical & Engineering Data*, 61(1), 247-254.
28. Manov, G.G., Bates, R. G., Hamer, W. J., & Acree, S. F. (1943). Values of the constants in the Debye - Hückel equation for activity coefficients I. *Journal of the American Chemical Society*, 65(9), 1765-1767.
29. Liang, Z.H., Rongwong, W., Liu, H., Fu, K., Gao, F.,...&Nath, D, (2015), Recent progress and new developments in post-combustion carbon-capture technology with amine based solvents. *International Journal of Greenhouse Gas Control*, 40, 26-54.
30. Rochelle, G., Chen, E., Freeman, S., Van Wagener, D., Xu, Q., & Voice, A. (2011). Aqueous piperazine as the new standard for CO<sub>2</sub> capture technology. *Chemical engineering journal*, 171(3), 725-733.
31. Rochelle, G.T. (2009). Amine scrubbing for CO<sub>2</sub> capture. *Science*, 325(5948), 1652-1654.
32. Versteeg, G. F., Van Dijck, L.A., & van Swaij, W.P.M. (1996). On the kinetics between CO<sub>2</sub> and alkanolamines both in aqueous and non-aqueous solutions. An overview. *Chemical Engineering Communications*, 144(1), 113-158.
33. Aboaba, A. J. (2017). Reaction kinetics and dissociation constants ( $pK_a$ ) of tertiary alkanolamines for carbon capture. (Master's dissertation, University of Regina)
34. Hamborg, E.S., & Versteeg, G.F. (2009). Dissociation constants and thermodynamic properties of alkanolamines. *Energy Procedia*, 1(1), 1213-1218.
35. Kielland, J. (1937). Individual activity coefficients of ions in aqueous solutions. *Journal of the American Chemical Society*, 59(9), 1675-1678.
36. Harned, H.S., Hamer, W.J. (1933). The ionization constant of water and the dissociation of water in potassium chloride solutions from electromotive forces of cells without liquid junction. *Journal of the American Chemical Society*, 55(6), 2194-2206.
37. Pérez -Salado Kamps, Á. & Maurer, G. (1996). Dissociation constant of N-methyldiethanolamine in aqueous solution at temperatures from 278 K to 368 K. *Journal of Chemical & Engineering Data*, 41(6), 1505-1513.

38. Littel, R.J., Bos, M., & Knoop, G. J. (1990). Dissociation constants of some alkanolamines at 293, 303, 318, and 333 K. *Journal of Chemical & Engineering Data*, 35(3), 276-277.
39. Sumon, K. Z., Henni, A., & East, A. L. (2012). Predicting pK<sub>a</sub> of amines for CO<sub>2</sub> capture: computer versus pencil-and-paper. *Industrial & Engineering Chemistry Research*, 51(37), 11924-11930.
40. Qian, J., Sun, R., Sun, S., & Gao, J. (2016). Computer-free group-addition method for pK<sub>a</sub> prediction of 73 amines for CO<sub>2</sub> capture. *Journal of Chemical & Engineering Data*, 62(1), 111-122.
41. Shields, G.C., & Seybold, P.G. (2013). *Computational approaches for the prediction of pK<sub>a</sub> values*. CRC Press.
42. Rahman, M. A., Muniyandi, R. C., Islam, K. T., & Rahman, M. M. (2019, October). Ovarian Cancer Classification Accuracy Analysis Using 15-Neuron Artificial Neural Networks Model. In *2019 IEEE Student Conference on Research and Development (SCOReD)* (pp. 33-38). IEEE.
43. Khalili, F. (2008). pK<sub>a</sub> determination of alkanolamines: Experimental and theoretical approaches (Master's dissertation, University of Regina)
44. Sumon, K.Z. (2013). Quantum-mechanical and thermodynamic study of amines and ionic liquids for CO<sub>2</sub> capture (Doctoral dissertation, University of Regina)
45. Yegnanarayana, B. (2009). *Artificial neural networks*. New Delhi: PHI Learning Pvt. Ltd.
46. Ahmadloo, Z. (2016). Predictability of carbon dioxide and ethane solubility in ionic liquids: A simulation approach (Master's dissertation, University of Regina)
47. Artemenko, N., Artemenko, N. V., Baskin, I. I., Palyulin, V. A., & Zefirov, N. S. (2001). Prediction of physical properties of organic compounds using artificial neural networks within the substructure approach. In *Doklady Chemistry*, 381(1-3), 317-320.
48. Habibi-Yangjeh, A., Danandeh-Jenagharad, M., & Nooshyar, M. (2005). Prediction acidity constant of various benzoic acids and phenols in water using linear and nonlinear QSPR models. *Bulletin-Korean Chemical Society*, 26(12), 2007.
49. Kauffman, G.W., & Jurs, P.C. (2001). Prediction of surface tension, viscosity, and thermal conductivity for common organic solvents using quantitative structure - property relationships. *Journal of Chemical Information and Computer Sciences*, 41(2), 408-418.

50. Zhang, R., Liu, S., Liu, M., & Hu, Z. (1997). Neural network-molecular descriptors approach to the prediction of properties of alkenes. *Computers & Chemistry*, 21(5), 335-341.
51. Mandal, B.P., Kundu, M., & Bandyopadhyay, S.S. (2003). Density and viscosity of aqueous solutions of (N-methyldiethanolamine + monoethanolamine), (N-methyldiethanolamine + diethanolamine), (2-amino-2-methyl-1-propanol + monoethanolamine), and (2-amino-2-methyl-1-propanol + diethanolamine). *Journal of Chemical & Engineering Data*, 48(3), 703-707.
52. Muhammad, A., Mutalib, M. I. A., Murugesan, T., & Shafeeq, A. (2008). Density and excess properties of aqueous N-methyldiethanolamine solutions from (298.15 to 338.15) K. *Journal of Chemical & Engineering Data*, 53(9), 2217- 2221.
53. Blanco, A., García -Abuín, A., Gómez-Díaz, D., Navaza, J. M., & Villaverde, O. L. (2013). Density, speed of sound, viscosity, surface tension, and excess volume of N-ethyl-2-pyrrolidone + ethanolamine (or diethanolamine or triethanolamine) from T = (293.15 to 323.15) K. *Journal of Chemical & Engineering Data*, 58(3), 653-659.
54. Blanco, A., García -Abuín, A., Gómez -Díaz, D., & Navaza, J. M. (2012). Density, speed of sound, viscosity, refractive index, and excess volume of N-methyl-2-pyrrolidone + ethanol (or water or ethanolamine) from T = (293.15 to 323.15) K. *Journal of Chemical & Engineering Data*, 56(3), 646-651.
55. Moosavi, M., Sisco, C. J., Rostami, A. A., & Vargas, F. M. (2017). Thermodynamic properties and CO<sub>2</sub> solubility of monoethanolamine + diethylenetriamine/ aminoethyl ethanolamine mixtures: Experimental measurements and thermodynamic modeling. *Fluid Phase Equilibria*, 449, 175-185.
56. Vázquez, G., Alvarez, E., Navaza, J. M., Rendo, R., & Romero, E. (1997). Surface tension of binary mixtures of water + monoethanolamine and water + 2- amino-2-methyl-1-propanol and tertiary mixtures of these amines with water from 25 °C to 50 °C. *Journal of Chemical & Engineering Data*, 42(1), 57-59.
57. Rayer, A.V., Kadiwala, S., Narayanaswamy, K., & Henni, A. (2010). Volumetric properties, viscosities, and refractive indices for aqueous 1-amino-2-propanol (monoisopropanolamine (MIPA)) Solutions from (298.15 to 343.15) K. *Journal of Chemical & Engineering Data*, 55(12), 5562-5568.
58. Narayanaswamy, K., Rayer, A. V., Kadiwala, S., & Henni, A. (2012). Volumetric properties, viscosities, refractive indices and surface tensions for (dimethyl propanol amine (DMPA) + water) mixtures from 298.15 K to 343.15 K. *Thermochimica Acta*, 543, 218-225.

59. Li, J., Mundhwa, M., Tontiwachwuthikul, P., & Henni, A. (2007). Volumetric properties, viscosities, and refractive indices for aqueous 2-(methylamino)ethanol solutions from (298.15 to 343.15) K. *Journal of Chemical & Engineering Data*, 52(2), 560-565.
60. Kumar, A., Solanki, A., Nguyen, W. H. C. H., & Henni, A. (2020). Determination and Prediction of Dissociation Constants and Related Thermodynamic Properties for 2-(Butylamino) ethanol, m-Xylylenediamine, 3-Picolylamine, Isopentylamine, and 4-(Aminoethyl)-piperidine. *Journal of Chemical & Engineering Data*, 65(11), 5437-5442.
61. Ghulam, M., Mohd, S. A., Azmi, B. M., & Faizan, A. (2013). Volumetric properties, viscosities and refractive indices of aqueous solutions of 2-amino-2-methyl-1-propanol (AMP). *Res. J. Chem. Environ*, 17(9), 22-31.
62. Álvarez, E., Cerdeira, F., Gómez-Díaz, D., & Navaza, J. M. (2010). Density, speed of sound, isentropic compressibility, and excess volume of binary mixtures of 1-amino-2-propanol or 3-amino-1-propanol with 2-amino-2-methyl-1-propanol, diethanolamine, or triethanolamine from (293.15 to 323.15) K. *Journal of Chemical & Engineering Data*, 55(7), 2567-2575.
63. Spasojević, V.D., Šerbanović, S. P., Djordjević, B. D., & Kijevčanin, M. L. (2012). Densities, viscosities, and refractive indices of aqueous alkanolamine solutions as potential carbon dioxide removal reagents. *Journal of Chemical & Engineering Data*, 58(1), 84-92.
64. Tseng, Y. M., & Thompson, A.R. (1964). Densities and refractive indices of aqueous monoethanolamine, diethanolamine, triethanolamine. *Journal of Chemical & Engineering Data*, 9(2), 264-267.
65. Vázquez, G., Alvarez, E., Rendo, R., Romero, E., & Navaza, J. M. (1996). Surface tension of aqueous solutions of diethanolamine and triethanolamine from 25 °C to 50 °C. *Journal of Chemical & Engineering Data*, 41 (4), 806-808.
66. Bower, V.E., Robinson, R.A., & Bates, R.G. (1962). Acidic dissociation constant and related thermodynamic quantities for diethanolammonium ion in water from 0 to 50°C. *J. Res. Natl. Bur. Stand. A*, 66, 71-75.
67. Omrani, A., Rostami, A.A., & Mokhtary, M. (2010). Densities and volumetric properties of 1,4-dioxane with ethanol, 3-methyl-1-butanol, 3-amino-1-propanol and 2-propanol binary mixtures at various temperatures. *Journal of Molecular Liquids*, 157(1), 18-24.
68. Álvarez, E., Cancela, Á., Maceiras, R., Navaza, J. M., & Táboas, R. (2003). Surface tension of aqueous binary mixtures of 1-amino-2-propanol and 3-amino-1-propanol, and aqueous ternary mixtures of These amines with diethanolamine,

- triethanolamine, and 2-amino-2-methyl-1-propanol from (298.15 to 323.15) K. *Journal of Chemical & Engineering Data*, 48(1), 32-35.
69. Saravanakumar, K., Baskaran, R., & Kubendran, T.R. (2011). Thermophysical properties of acetophenone with N,N-dimethylethanolamine or with N,N-diethylethanolamine at temperatures of (303.15, 313.15 and 323.15) K and pressure of 0.1 MPa. *Journal of Solution Chemistry*, 40(6), 955-967.
  70. Iloukhani, H., & Rakhshi, M. (2009). Excess molar volumes, viscosities, and refractive indices for binary and ternary mixtures of {cyclohexanone (1) + N,N-dimethylacetamide (2)+N,N-diethylethanolamine (3)} at (298.15, 308.15, and 318.15)K. *Journal of Molecular Liquids*, 149(3), 86-95.
  71. DiGuilio, R.M., Lee, R. J., Schaeffer, S. T., Brasher, L. L., & Teja, A. S. (1992). Densities and viscosities of the ethanolamines. *Journal of Chemical and Engineering Data*, 37(2), 239-242.
  72. Kinart, C.M., Kinart, W.J., & Chęcińska-Majak, D. (2002). Density, relative permittivity, and viscosity at various temperatures for 2-methoxyethanol + propylamine mixtures. *Journal of Chemical & Engineering Data*, 47(6), 1537-1539.
  73. Babak, S.F., Airapetova, R., & Udovenko, V. (1950). Study of systems formed by formic acid. *Zh. Obshch. Khim*, 20(5), 770-773.
  74. Álvarez, E., Gómez-Díaz, D., La Rubia, M. D., & Navaza, J. M. (2007). Surface tension of aqueous binary mixtures of 2-(methylamino)ethanol and 2-(ethylamino)ethanol and aqueous ternary mixtures of these amines with triethanolamine or N-methyldiethanolamine from (293.15 to 323.15) K. *Journal of Chemical & Engineering Data*, 53(1), 318-321.
  75. Álvarez, E., Gómez-Díaz, D., La Rubia, M. D., & Navaza, J. M. (2006). Densities and viscosities of aqueous ternary mixtures of 2-(methylamino)ethanol and 2-(ethylamino)ethanol with diethanolamine, triethanolamine, N-methyldiethanolamine, or 2-amino-1-methyl-1-propanol from 298.15 to 323.15 K. *Journal of Chemical & Engineering Data*, 51(3), 955-962.
  76. Lampreia, I.M., Santos, Â. F., Barbas, M. J. A., Santos, F. J., & Matos Lopes, M. L. (2007). Changes in aggregation patterns detected by diffusion, viscosity, and surface tension in water + 2-(diethylamino)ethanol mixtures at different temperatures. *Journal of Chemical & Engineering Data*, 52(6), 2388-2394.
  77. Kinart, C.M., Kinart, W. J., Chęcińska-Majak, D., & Ćwiklińska, A. (2003). Refractive properties of binary mixtures containing 2-methoxyethanol and n-butylamine, isobutylamine, sec-butylamine and tert-butylamine. *Physics and Chemistry of Liquids*, 41(4), 383-389.

78. Wang, J., Du, H., Liu, H., Yao, X., Hu, Z., & Fan, B. (2007). Prediction of surface tension for common compounds based on novel methods using a heuristic method and support vector machine. *Talanta*, 73(1), 147-156.
79. Pal, A., Kumar, A., & Kumar, H. (2006). Volumetric, acoustic, viscometric, and spectroscopic properties for binary mixtures of alkoxypropanol with mono, di- and tri-alkylamines at a temperature of 298.15K. *The Journal of Chemical Thermodynamics*, 38(10), 1227-1239.
80. Blanco, A., García -Abuín, A., Gómez -Díaz, D., & Navaza, J. M. (2017). Density, speed of sound, viscosity and surface tension of 3-dimethylamino-1-propylamine+ water, 3-amino-1-propanol + 3-dimethylamino-1-propanol, and (3-Amino-1-propanol + 3-dimethylamino-1-propanol) + water from T = (293.15 to 323.15) K. *Journal of Chemical & Engineering Data*, 62(8), 2272-2279.
81. Tissier, C., & Barillie, P.(1969). Acidity constants and thermodynamic functions of acids conjugated with some propanediamines. *Comptes Rendus Hebdomadaires des Séances De L'Académie des Sciences Série C*, 268(22), 1953.
82. Razavizadeh, S.A., Sheikh, S., & Nassaj Gerowgi, Z. (2017). Measurement of thermophysical properties of pure and mixture of alkanolamines from 288.15-323.15 K. *physical chemistry research*, 5(2), 269-279.
83. Philip, F. & Nath, D. & Sibilla, K. & Henni, A. (2019). Volumetric properties, viscosities and refractive indices of {3-diethylamino propylamine (DEAPA) + water} system from 293.15 K to 343.15 K. *The Journal of Chemical Thermodynamics*. 142. 105978. 10.1016/j.jct.2019.105978.

## Appendix A: Experimental Determination of Physical Properties of Amines

### Appendix A-1: Density Measurement

An Anton Paar DMA-4500 density meter was used to measure the densities for the eight amines. For calibrating the density meter, firstly we had to check the atmospheric pressure to make sure that it matches the laboratory conditions following which we needed to perform Air and Water (double distilled) checks at a specified temperature. Then we need to make sure that the obtained values were within  $5E-5$  g/ml of the desired values. The experimental density of MEA was verified with literature values from data published by Vázquez et al. [56] with deviations of 0.003 and 0.002 g/ml for two different temperatures respectively. All the experimental values are listed in Table A-1.

Table A-1. Density values for the studied amines

Chemical	Density (g/ml)				
	298.15K	303.15K	308.15K	313.15K	323.15K
Monoethanolamine	1.01172	1.00777	1.00381	0.99983	0.99183
3-(Diethylamino)propylamine	0.82318	0.81890	0.81463	0.81036	0.80179
1,3-Diaminopentane	0.85710	0.85285	0.84859	0.84433	0.83576
3-Butoxypropylamine	0.84626	0.84188	0.83749	0.83310	0.82426
2-(Methylamino)ethanol	0.93651	0.93263	0.92872	0.92479	0.91687
Bis(2-methoxyethyl) amine	0.91113	0.90664	0.90214	0.89762	0.88857
$\alpha$ -Methylbenzylamine	0.95294	0.94864	0.94432	0.93999	0.93128
2-Aminoheptane	0.76062	0.75643	0.75221	0.74797	0.73946
3-Amino-1-phenylbutane	0.92301	0.91898	0.91501	0.91104	0.90305

## Appendix A-2: Viscosity Measurement

Cannon-Fenske viscometers were used to measure the viscosity of all eight amines. A water bath (model CT500) from Cannon Instrumental Company was used to control and set the desired temperatures and an external thermometer Cole Parmer resistance (model H-01158-65) with an accuracy of 0.001K was used to note temperature reading. A digital stopwatch from Fisher Scientifics was used to record time and the uncertainty was 0.01s. Firstly, the kinematic viscosity was obtained using Poiseuille's law written in Equation A-2.1. By multiplying the kinematic viscosity and density, the dynamic viscosity was obtained.

$$V = k_1 t - \frac{k_2}{t} \nu \quad \text{Eqn. A-2.1}$$

We validated the results of MEA by comparing its values to literature data published by Mandal [51] and the maximum observed deviation was 0.43 mPa·s. The experimental results are listed in Table A-2.1.

Table A-2.1 Viscosities of the studied amines

Chemical	Dynamic Viscosity (mPa·s)				
	298.15K	303.15K	308.15K	313.15K	323.15K
Monoethanolamine	18.66	15.55	12.55	10.24	6.88
3-(Diethylamino)propylamine	1.12	1.01	0.928	0.851	0.726
1,3-Diaminopentane	1.90	1.69	1.52	1.28	1.06
3-Butoxypropylamine	1.50	1.31	1.19	1.09	0.924
2-(Methylamino)ethanol	10.63	8.57	7.06	6.06	4.34
Bis(2-methoxyethyl) amine	1.15	1.07	0.994	0.922	0.783
$\alpha$ -Methylbenzylamine	1.89	1.69	1.44	1.311	1.09
2-Aminoheptane	0.821	0.752	0.699	0.646	0.563
3-Amino-1-phenylbutane	2.66	2.35	2.10	1.88	1.55

### Appendix A-3: Refractive Index Measurement

To measure the refractive index Atago RX-5000 $\alpha$  was used, and for validating the refractometer the measured values of water were compared with the literature [83] and the uncertainty was 0.00003. The experimental results are listed in Table A-3.1.

Table A-3.1 Refractive index of the studied amines

Chemical	Refractive Index				
	298.15K	303.15K	308.15K	313.15K	323.15K
Monoethanolamine	1.4535	1.4519	1.4505	1.4446	1.43980
3-(Diethylamino)propylamine	1.43999	1.43787	1.43567	1.43335	1.42868
1,3-Diaminopentane	1.45042	1.44808	1.44572	1.44344	1.43876
3-Butoxypropylamine	1.42474	1.42247	1.42018	1.41789	1.41322
2-(Methylamino)ethanol	1.43701	1.43513	1.43303	1.43099	1.42719
Bis(2-methoxyethyl) amine	1.41821	1.41605	1.41394	1.41176	1.40739
$\alpha$ -Methylbenzylamine	1.52412	1.52151	1.51917	1.51659	1.51161
2-Aminoheptane	1.41633	1.41407	1.41175	1.40930	1.40430
3-Amino-1-phenylbutane	1.51126	1.50865	1.50668	1.50483	1.50003

## Appendix A-4: Sound Velocity Measurement

Anton Paar DSA-4500 density meter was used to measure the sound velocity. The calibration process was the same as for density measurement, but the sound module was operated separately and used for the experimental process. The experimental results are listed in Table A-4.1.

Table A-4.1 Sound velocity of the studied amines

Chemical	Sound Velocity				
	298.15K	303.15K	308.15K	313.15K	323.15K
Monoethanolamine	1718.27	1702.06	1686.19	1670.45	1638.65
3-(Diethylamino)propylamine	1343.68	1333.49	1320.88	1305.47	1277.50
1,3-Diaminopentane	1491.65	1472.99	1453.88	1435.04	1395.53
3-Butoxypropylamine	1331.75	1317.35	1302.46	1288.15	1257.70
2-(Methylamino)ethanol	1469.59	1455.97	1440.54	1425.15	1396.37
Bis(2-methoxyethyl)amine	1273.78	1259.39	1244.30	1234.62	1202.62
$\alpha$ -Methylbenzylamine	1482.89	1473.81	1461.42	1446.26	1411.66
2-Aminoheptane	1277.40	1271.53	1257.26	1240.32	1199.32
3-Amino-1-phenylbutane	1555.62	1538.69	1520.93	1502.51	1465.26

## Appendix B: Weights and Bias of different layers in ANN

### Appendix B-1: Weights and bias for the model with all input parameters.

On training, the model with the entire feature set has resulted in 40 neurons in the first hidden layer. As we have a total of 10 input features, we would be having a 10\*40 matrix of weights with a column describing the bias. The association between each input parameter and each neuron in the hidden layer is outlined in the hidden layer.

Table B-1.1 Weights and biases of the first hidden layer

Temperature	Molecular weight	Number of C	Number of H	Number of N	Number of O	Refractive index	Sound velocity	Density	Viscosity	Bias
-0.1606	0.0418	-0.2179	0.1791	-0.5387	0.5581	-0.0116	0.5601	0.3960	0.5408	0.1280
-0.0019	0.2824	-0.4485	0.6275	-0.4088	-0.0983	0.2342	0.2044	-0.2735	-0.9534	0.4230
0.3512	0.5736	-0.4307	-0.0813	-0.7615	-0.0966	0.6547	0.1445	-0.7132	-0.5333	0.3857
-0.7657	0.4059	0.2351	-0.1342	0.4731	0.5649	-0.5287	0.4273	-0.5889	0.4599	0.0970
-0.5625	0.6416	-0.0182	-0.5174	0.3660	0.6449	-0.1326	-0.6361	-0.2539	0.2892	-0.1645
0.0953	0.3919	-0.3118	0.3992	0.7698	-0.6674	-0.5810	-0.1775	-0.4318	-0.7450	0.1681
0.2029	0.7125	-0.5716	0.0432	-0.3829	0.6687	-0.4168	0.2658	0.2181	0.0705	-0.1781
-0.3264	-0.7266	0.3055	0.0234	-0.7161	0.0598	-0.5198	0.0999	0.6816	-0.4716	0.1862
-0.6917	0.3358	-0.2423	-0.3921	0.5583	0.2305	0.3588	-0.6494	0.4169	-0.7451	0.1513
-0.5985	-0.8256	-0.0713	0.6598	-0.2951	-0.1735	-0.0084	0.6206	0.4261	0.3258	-0.2165
0.7704	0.3803	0.4634	0.6663	-0.4879	0.6356	0.4890	0.1110	0.2620	-0.2092	0.0304
-0.3404	-0.5674	-0.7932	-0.5772	-0.4899	-0.2049	-0.5343	0.2947	-0.1619	-0.1266	0.0807
-0.0338	-0.6166	-0.3253	-0.7251	0.0677	0.6614	0.4311	-0.7018	-0.6937	-0.4153	0.1659
-0.2682	-0.5091	0.0480	0.3170	-0.7225	0.8834	-0.3158	0.0101	-0.4100	-0.1235	0.2524
0.2565	-0.1078	0.3414	-0.4316	-0.2166	0.0072	-0.7935	0.5236	-0.0566	-0.4636	-0.0757
0.3958	0.4307	-0.0701	0.2972	-0.6833	0.5825	0.6117	-0.5569	-0.6424	-0.5044	0.2795
0.0319	0.0469	-0.3511	0.0314	-0.9649	0.7494	0.4980	0.2465	-0.7343	0.5067	0.2693
-0.5768	-0.2701	0.6151	-0.5232	0.0859	-0.7951	-0.0321	0.0401	0.2094	-0.0761	0.3236
-0.1144	-0.7453	-0.0239	0.6069	0.8351	-0.2969	-0.0053	0.0238	-0.1657	0.5311	0.1203
-0.3066	0.4596	-0.4190	0.0733	-0.7205	-0.9337	-0.1272	-0.2780	-0.3781	0.2868	0.4707
-0.7033	-0.3322	-0.7593	0.0392	-0.3011	0.8993	0.5743	-0.6363	-0.5388	-0.5341	0.1583
-0.2757	0.5471	-0.7170	-0.3693	-0.8787	0.6861	-0.6731	-0.6895	0.0206	-0.1790	0.3536

0.0430	-0.5891	-0.5039	-0.0625	-0.5739	-0.1442	-0.3621	0.2378	-0.2223	-0.0527	0.3039
0.0180	0.8456	-0.2889	-0.6364	0.6036	-0.0969	-0.3055	0.2153	-0.3660	0.1361	0.1386
0.4003	0.1114	0.5461	-0.3675	0.6447	-0.0693	-0.7118	0.6243	-0.0737	0.0206	0.3567
0.2454	-0.4345	0.3552	0.4435	-0.8293	0.3049	-0.3266	-0.6133	-0.5094	-0.0145	-0.1643
-0.3604	0.1635	0.4420	0.7140	0.8929	0.0178	-0.2349	-0.6850	0.2051	0.4970	0.1628
0.3333	0.0583	0.3531	-0.1965	-0.3599	0.5106	-0.2346	-0.7218	0.7650	-0.3121	0.3366
-0.4641	-0.4724	-0.5901	0.2899	-0.0581	-0.5267	-0.3159	-0.8717	-0.0177	-0.0139	0.1253
0.1067	-0.4578	-0.2740	0.2515	-0.7895	-0.2120	0.1888	-0.3705	0.6872	-0.1911	0.3330
-0.3392	-0.1498	0.3646	0.6204	-0.1839	0.6582	-0.3199	0.1551	0.3568	0.1923	0.1583
0.4965	0.5742	-0.3691	0.1134	-0.0984	-0.8393	-0.8090	-0.2186	-0.6202	0.1156	0.2307
0.6700	0.2042	-0.0350	0.3204	0.3162	0.4469	-0.8651	0.5723	0.0352	0.3410	-0.2331
0.1773	-0.5900	0.4932	0.3290	-0.4802	-0.3170	0.5759	0.5560	-0.6513	-0.9507	0.3155
-0.2870	-0.0699	-0.0866	-0.2916	-0.1423	0.3922	0.7709	0.0266	-0.4360	0.1056	-0.1400
0.3352	-0.3374	-0.7176	-0.3203	0.6644	-0.0147	0.3215	0.2830	-0.7252	0.4149	0.3521
0.0020	-0.2064	-0.5518	-0.0655	0.2919	-0.6655	-0.6246	-0.6007	0.7581	0.5035	-0.1730
0.7213	-0.0464	0.2616	-0.7370	0.0446	-0.4197	-0.6358	-0.5214	-0.4455	0.3504	0.1515
0.0745	0.7063	0.3609	0.0959	-0.1461	-0.2016	-0.1824	0.7324	0.1838	-0.7503	0.2346
-0.7435	-0.4516	0.6738	-0.1484	-0.1391	0.3766	0.5637	0.3620	-0.5014	-0.2568	0.1497

Based on the introduction of the second hidden layer with 39 neurons, the weights and bias have been calculated. This matrix was of dimension 40x39. Table B-1.2 contains this information and can be found at the following google drive [link 1](#).

The weights and biases of the neurons connected from the second hidden layer to the output layer would be of a 39x1 dimension represented in Table B-1.3 which can be found at the following google drive [link 2](#).

## Appendix B-2: Weights and bias for the model with optimized inputs.

Training the model with optimized parameters in which the Sound Velocity and Molecular weight were eliminated resulting in a highly scalable and less complex model, which had a good prediction accuracy. The weights and biases were reported in the following Table and links.

Table B-2.1 Weights and bias of first hidden layer

Temperature	Molecular Weight	Number of C	Number of H	Number of N	Number of O	Density	Viscosity	Bias
-1.12E-01	6.35E-01	-1.87E-01	4.64E-01	1.03E-01	2.24E-01	1.63E-04	-1.05E-01	-1.16E-01
6.15E-02	-3.45E-01	-8.29E-01	-1.80E-01	-4.87E-01	-2.35E-01	5.33E-02	-3.13E-01	1.33E-01
5.46E-01	-9.27E-02	6.76E-01	2.88E-01	-6.07E-01	4.30E-01	-4.68E-01	-5.56E-01	1.20E-01
9.27E-02	5.84E-01	-1.07E-01	5.23E-01	-4.25E-01	-4.34E-01	-4.75E-01	5.57E-01	-1.09E-01
1.49E-01	-5.44E-01	6.04E-01	4.29E-01	4.62E-01	-4.95E-01	-2.20E-01	-1.08E+00	3.01E-01
5.76E-01	2.66E-01	-5.99E-01	8.54E-02	-4.17E-01	5.11E-01	-3.40E-01	8.66E-01	2.32E-01
5.14E-01	5.38E-01	4.00E-01	5.43E-01	-2.44E-01	4.39E-01	-5.13E-01	3.05E-01	1.07E-01
5.63E-02	2.17E-01	4.33E-01	5.61E-01	5.30E-01	-1.89E-01	-3.63E-01	4.12E-01	2.37E-01
4.65E-01	-3.00E-01	1.16E-01	7.32E-01	3.86E-01	-8.81E-01	3.44E-01	4.82E-01	-5.31E-02
7.42E-01	3.28E-01	-6.44E-01	7.12E-01	4.06E-01	-8.01E-01	-1.24E-01	-3.98E-01	1.85E-01
2.28E-01	8.76E-01	6.16E-01	8.75E-01	4.00E-02	3.59E-01	-8.72E-01	6.41E-01	-2.10E-01
1.09E-01	-7.28E-01	2.79E-01	5.03E-02	-1.20E+00	-3.28E-02	3.78E-01	-2.24E-02	3.55E-01
-5.20E-01	6.77E-01	-2.61E-02	-6.91E-01	8.76E-01	-9.84E-01	3.94E-02	6.51E-01	1.74E-01
5.31E-02	8.79E-01	9.90E-01	-8.19E-02	-3.54E-01	-1.23E-01	-2.71E-01	7.15E-01	1.84E-01
2.42E-01	8.38E-01	-6.45E-01	9.18E-01	6.95E-01	4.07E-01	-2.74E-01	8.45E-01	-1.89E-01
8.90E-02	4.07E-01	6.35E-02	5.08E-01	5.60E-01	-4.59E-01	-4.79E-01	-8.58E-01	2.15E-01
2.64E-01	-3.41E-01	-6.56E-01	-5.09E-01	1.73E-01	3.70E-01	-4.62E-01	-4.94E-01	1.53E-01
7.85E-01	-3.59E-01	5.91E-01	1.13E-01	3.09E-01	1.57E-01	6.12E-01	-3.84E-01	1.08E-01
1.41E-01	-1.14E-02	7.49E-01	-7.06E-01	-6.96E-01	3.82E-01	6.78E-01	-2.40E-01	2.20E-01
3.10E-01	-6.27E-01	-3.26E-01	-1.63E-01	-4.58E-01	-4.79E-01	-7.15E-01	1.69E-02	3.60E-01
4.94E-01	2.62E-03	5.36E-01	-6.17E-02	-3.08E-02	5.48E-01	-6.16E-01	-7.89E-01	3.11E-01
7.64E-01	-1.26E-01	2.09E-01	9.11E-01	-5.84E-01	-7.30E-01	6.67E-01	-2.21E-01	-2.15E-01
1.17E-01	1.04E-01	3.70E-01	-9.41E-01	8.75E-01	2.05E-01	3.03E-01	1.62E-01	-3.29E-02
6.09E-02	-1.35E-01	-1.92E-01	3.79E-01	-8.31E-01	6.28E-01	6.99E-01	-6.93E-01	2.67E-01
-6.55E-01	7.36E-01	-4.25E-01	3.77E-01	2.13E-01	-3.71E-01	-3.42E-02	-6.67E-01	3.87E-01

6.89E-01	-5.66E-01	6.20E-01	-2.86E-01	-3.52E-01	-2.70E-01	5.16E-01	5.08E-01	-1.35E-01
-6.73E-01	2.03E-01	5.10E-01	-1.97E-01	-9.72E-01	-6.39E-01	6.42E-01	-6.94E-01	2.78E-01
2.17E-01	5.48E-01	-3.09E-01	6.21E-02	1.74E-01	-6.55E-01	2.07E-01	4.69E-01	-3.03E-02
-6.97E-01	4.66E-01	1.49E-01	-3.03E-01	7.72E-01	9.05E-01	-7.43E-01	-6.09E-01	1.54E-01
1.53E-01	-4.81E-01	-6.96E-01	8.16E-01	-7.64E-01	4.78E-01	2.93E-01	7.57E-01	1.91E-01
9.45E-02	-5.13E-01	-2.31E-01	7.20E-01	9.50E-01	-5.22E-01	-5.60E-01	6.87E-01	8.59E-02
2.47E-01	-2.84E-01	-2.65E-01	6.38E-01	-7.15E-01	-4.95E-01	-4.65E-01	-5.65E-01	5.16E-01
3.65E-02	-7.15E-01	6.10E-01	8.26E-01	-3.67E-01	-8.25E-01	-1.36E-01	8.58E-01	-2.32E-01
5.21E-01	2.59E-01	-8.06E-01	1.78E-01	1.46E-01	3.02E-01	-5.66E-01	3.80E-01	-3.20E-01
-2.94E-01	-7.26E-01	7.99E-01	3.32E-01	-3.57E-02	3.26E-02	2.62E-01	4.75E-01	2.34E-01
4.61E-02	-5.90E-01	9.10E-01	-7.34E-01	-6.31E-01	5.02E-01	-2.02E-01	5.71E-01	3.06E-01
1.19E-01	5.19E-01	6.00E-01	-7.23E-01	-3.86E-01	8.40E-01	-3.78E-01	-2.76E-01	2.42E-01
9.02E-01	4.59E-01	-7.77E-01	2.78E-01	-1.63E-01	1.61E-01	-3.14E-01	6.06E-01	-2.49E-01
-2.67E-01	-8.04E-02	1.35E-01	1.86E-01	-7.96E-01	4.83E-01	-7.49E-01	-6.08E-01	6.13E-01

Based on the introduction of the second hidden layer with 39 neurons, the weights and bias have been calculated. This matrix is of dimension 40x39. Table B-2.2 containing this information can be found at the following google drive [link 3](#).

The weights and bias of the neurons connected from the second hidden layer to the output layer would be of a 39x1 dimension represented in Table B-2.3 which can be found at the following google drive [link 4](#).